

University of New Hampshire

University of New Hampshire Scholars' Repository

Master's Theses and Capstones

Student Scholarship

Fall 2012

An empirical study of image processing methods for land cover classification and forest cover change detection in Northeastern Oregon's timber resource-dependent communities (1986-2011)

Michael James Campbell
University of New Hampshire, Durham

Follow this and additional works at: <https://scholars.unh.edu/thesis>

Recommended Citation

Campbell, Michael James, "An empirical study of image processing methods for land cover classification and forest cover change detection in Northeastern Oregon's timber resource-dependent communities (1986-2011)" (2012). *Master's Theses and Capstones*. 720.
<https://scholars.unh.edu/thesis/720>

This Thesis is brought to you for free and open access by the Student Scholarship at University of New Hampshire Scholars' Repository. It has been accepted for inclusion in Master's Theses and Capstones by an authorized administrator of University of New Hampshire Scholars' Repository. For more information, please contact Scholarly.Communication@unh.edu.

**AN EMPIRICAL STUDY OF IMAGE PROCESSING METHODS FOR LAND
COVER CLASSIFICATION AND FOREST COVER CHANGE DETECTION IN
NORTHEASTERN OREGON'S TIMBER RESOURCE-DEPENDENT
COMMUNITIES (1986-2011)**

BY

MICHAEL JAMES CAMPBELL

B.A. Geography, State University of New York at Geneseo, 2009

THESIS

**Submitted to the University of New Hampshire
in Partial Fulfillment of
the Requirements for the Degree of**

**Master of Science
in
Natural Resources**

September, 2012

UMI Number: 1521539

All rights reserved

INFORMATION TO ALL USERS

The quality of this reproduction is dependent upon the quality of the copy submitted.

In the unlikely event that the author did not send a complete manuscript and there are missing pages, these will be noted. Also, if material had to be removed, a note will indicate the deletion.

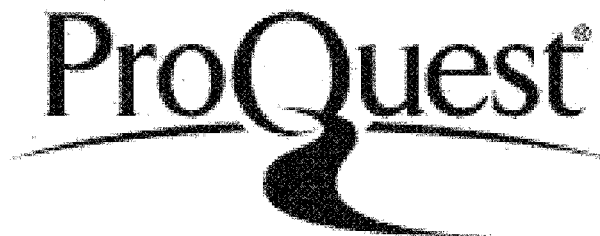


UMI 1521539

Published by ProQuest LLC 2012. Copyright in the Dissertation held by the Author.

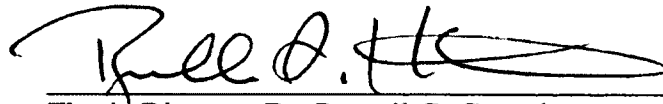
Microform Edition © ProQuest LLC.

All rights reserved. This work is protected against unauthorized copying under Title 17, United States Code.



ProQuest LLC
789 East Eisenhower Parkway
P.O. Box 1346
Ann Arbor, MI 48106-1346

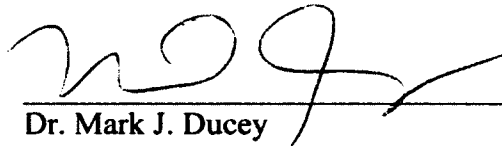
This thesis has been examined and approved.



Thesis Director, Dr. Russell G. Congalton
Professor of Remote Sensing and Geographic Information
Systems



Dr. Joel N. Hartter
Assistant Professor of Geography



Dr. Mark J. Ducey
Professor of Forest Biometrics and Management

7/25/12

Date

ACKNOWLEDGEMENTS

I would first like to thank the members of my graduate committee for all of their support throughout this process. Without their personal and professional guidance and leadership, this project would have not been possible. Specifically, I would like to thank my advisor, Dr. Russell Congalton, for not only providing me with the resources to complete my Master's research, but introducing me to the realm of remote sensing and for his consistent willingness to discuss every step in the process, no matter how seemingly insignificant. I would like to thank Dr. Joel Hartter for inviting me to join his research team on this exciting and meaningful project and for giving me the freedom and opportunity to explore my own research interests in a beautiful region of the country. I would also like to thank Dr. Mark Ducey, for his expertise in forestry and for teaching me about field methods, expanding my research toolbox beyond the confines of a computer screen.

I would be remiss not to thank my fellow students for all of their help, both inside the classroom and out. Not enough thanks can be given to Mrs. Meghan Graham MacLean, for being a constant springboard for ideas, for providing me with valuable insight on being a successful graduate student, and for being an outstanding person to share a research space with. Thank you to Mr. Daniel Maynard for his assistance in the field, his seemingly limitless understanding and ease of explaining statistics, and for helping me maintain a level of sanity in an otherwise insane set of circumstances. Thank you to Ms. Lucy Parham for her undying support and companionship, for giving me a life

outside of James Hall, and for being the wonderful, caring and kind woman that she is. I would also like to thank Ms. Michelle Robbins, whose hours of tireless work greatly facilitated the timely and effective completion of my research.

Last, but certainly not least, I would like to thank my family and friends for getting me to where I am today and providing me with endless love and support throughout all of my endeavors, academic and beyond.

This research was made possible through the financial assistance of the Department of Natural Resources and the Environment's teaching assistantship program funded by the University of New Hampshire and the United States Department of Agriculture's Disaster Resilience for Rural Communities program Grant #2010-67023-21705.

TABLE OF CONTENTS

ACKNOWLEDGEMENTS.....	iii
LIST OF FIGURES.....	vii
LIST OF TABLES.....	ix
ABSTRACT.....	xi
I. INTRODUCTION.....	1
Literature Review.....	3
Image Data.....	3
Image Pre-Processing	5
Segmentation Parameter Analysis and Land Cover Classification.....	11
Accuracy Assessment	19
Land Cover Change.....	21
Objectives.....	25
II. METHODS.....	27
Study Area.....	27
Reference Data.....	30
Image Data.....	32
Image Pre-Processing	34
Segmentation Parameter Analysis and Land Cover Classification.....	40
Accuracy Assessment	43
Land Cover Change.....	44

Change Detection.....	43
Change Classification.....	47
III. RESULTS.....	50
Segmentation Parameter Analysis and Land Cover Classification.....	50
Accuracy Assessment	60
Land Cover Change.....	63
IV. CONCLUSIONS.....	81
Segmentation Parameters.....	82
OBIA vs. Pixel-Based Classification	86
CART vs. Bayes.....	88
Accuracy Assessment	93
Change Detection.....	96
Forest Cover Change.....	100
LITERATURE CITED.....	105
APPENDICES.....	111
APPENDIX A: UNION AND BAKER COUNTY LAND OWNERSHIP TOTALS.....	112
APPENDIX B: CHANGE DETECTION ACCURACY ASSESSMENTS BY BAND.....	113
APPENDIX C: BAND 7 CHANGE DETECTION ACCURACY ASSESSMENTS BY THRESHOLD.....	116
APPENDIX D: LAND COVER AREA TOTALS.....	118

LIST OF FIGURES

Figure 1. eCognition's multiresolution segmentation parameters.....	15
Figure 2. Study area map, Union and Baker Counties, Oregon.....	28
Figure 3. Content of 23-band image.....	39
Figure 4. Change detection flowchart.....	44
Figure 5. C-CAP change classification flowchart.....	47
Figure 6. A subset scene of northwestern La Grande, Union County, OR segmented at scale parameters of 2 (left) and 20 (right).....	51
Figure 7. The effect of scale parameters on resultant segment size.....	52
Figure 8. The effect of scale parameters on variation in resultant segment size.....	53
Figure 9. A subset scene of northwestern La Grande, Union County, OR segmented at shape parameters of 0.0 (left) and 0.5 (right).....	54
Figure 10. Average overall accuracies of CO, CP, BO and BP across the range of scale parameters.....	55
Figure 11. Average overall accuracies of CO, CP, BO and BP across the range of shape parameters.....	56
Figure 12. 2011 land cover classification.....	59
Figure 13. Overall accuracies estimated using unit-based and area-based error matrices by scale parameter for CART (A) and Bayes (B).....	61
Figure 14. Overall accuracies estimated using unit-based and area-based error matrices by shape parameter for CART (A) and Bayes (B).....	62
Figure 15. The effect of segment size variation on differences in unit- and area-based error matrix accuracies.....	63
Figure 16. Example class-specific difference image value distributions.....	65

Figure 17. User's and producer's accuracies of change areas detected using different spectral and derivative bands.....	66
Figure 18. Kappa accuracy of change areas detected using different spectral and derivative bands.....	67
Figure 19. User's and producer's accuracies of change areas detected using band 7 at different standard deviation thresholds.....	69
Figure 20. Kappa accuracy of change areas detected using band 7 at different standard deviation thresholds.....	69
Figure 21. User's and producer's accuracies of change areas detected using band 7 at different time intervals.....	71
Figure 22. Kappa accuracy of change areas detected using band 7 at different time intervals.....	71
Figure 23. Total harvesting by 5-year interval broken down by land ownership Class.....	73
Figure 24. Percentage of total forested land removed by ownership by 5-year Interval.....	75
Figure 25. Total regeneration by 5-year interval broken down by land ownership Class.....	76
Figure 26. Percentage of total forested land regenerated by ownership by 5-year Interval.....	77
Figure 27. Ratio of forest harvesting to forest regeneration by 5-year interval broken down by ownership class.....	78
Figure 28. Long term total forest area projections based on 2006-2011 net forest harvesting percentages.....	80
Figure 29. Figurative image segmentations and sample unit assignment.....	84
Figure 30. Forest harvesting data in board footage from Oregon Department of Forestry, 1986-2010.....	103

LIST OF TABLES

Table 1. Land cover reference data.....	32
Table 2. Landsat 5 TM image dates.....	34
Table 3. Tasseled Cap transformation for Landsat 5 TM.....	38
Table 4. Error matrix of highest accuracy land cover classification before post-processing.....	57
Table 5. Error matrix of highest accuracy land cover classification after post-processing.....	58
Table 6. Principal components analysis of 10-band difference image with accordant eigenvalues and variance computations.....	64
Table 7. Mean and standard deviation of difference image values by land cover class.....	65
Table 8. Change detection error matrix for band 7, threshold 2 SD.....	68
Table 9. Change detection error matrix for band 7, threshold 1.75 SD.....	70
Table 10. Total harvesting by 5-year interval broken down by land ownership class.....	73
Table 11. Total forest area broken down by land ownership class and year.....	74
Table 12. Percentage of total forested land removed by ownership by 5-year interval.....	74
Table 13. Total regeneration by 5-year interval broken down by land ownership class.....	76
Table 14. Percentage of total forested land regenerated by ownership by 5-year interval.....	77
Table 15. Forest harvesting sustainability ratio by ownership class by 5-year interval.....	78

Table 16. Net forest harvesting by 5-year interval broken down by ownership class..... 79

ABSTRACT

AN EMPIRICAL STUDY OF IMAGE PROCESSING METHODS FOR LAND COVER CLASSIFICATION AND FOREST COVER CHANGE DETECTION IN NORTHEASTERN OREGON'S TIMBER RESOURCE-DEPENDENT COMMUNITIES (1986-2011)

By

Michael James Campbell

University of New Hampshire, September, 2012

A study was performed to evaluate remote sensing methods for classifying land cover and land cover change throughout a two-county area in Northeastern Oregon (1986-2011). In the past three decades, this region has seen significant changes in forest management – changes that can be readily identified from the synoptic perspective. This study employs an accuracy assessment-based empirical approach to test a number of advanced digital image processing techniques that have recently emerged in the field of remote sensing. The accuracies are assessed using traditional and area-based error matrices. It was determined that, for single-time land cover classification, Bayes pixel-based classification using samples created with segmentation parameters of scale 8 and shape 0.3 resulted in the highest overall accuracy. For land cover change detection, it was determined that Landsat 5 TM band 7 with a change threshold of 1.75 SD resulted in the highest accuracy for forest harvesting detection.

CHAPTER I

INTRODUCTION

Remote sensing technologies are unmatched in their ability to efficiently and accurately map the interaction between humans and the natural environment. At local, regional and global scales, the inventory and monitoring of Earth's natural resources is paramount to building towards a successful, sustainable future. Particularly in the last century, with increasing evidence of global climate change and the continuing expansion of human development, it is essential that the scientific community develop tools and methodologies to assess the changes that occur in the landscape over time. With technological and computational capacities on the rise, these tools and methodologies have the potential to greatly increase the efficiency and accuracy with which we can monitor land use and land cover changes. It is also likely, however, that with these increasing capacities comes increasing complexity. Especially in the realm of remote sensing, where newer, more advanced satellite imagery platforms are continually being launched, new analytical software packages are being developed and computer hardware is becoming exponentially more powerful, there is a seemingly limitless amount of remote sensing research and development to be done. While this is certainly an exciting prospect, it is also daunting for the discipline as a whole, as increasing avenues of specialization can result in increased methodological disagreement, decreased operational and data standards, and a general disconnect in theoretical frameworks. Given their

readily interpretable nature and broad applicability, the results of remote sensing studies are often used as a basis for interdisciplinary scientific inquiry (Roughgarden *et al.*, 1991) land management practices (Masser, 2001), and even legislative policymaking (Miller & Small, 2003). Accordingly, it is critical that the remote sensing community not only keep up with the advancing technologies by introducing new tools and methods, but continue to rigorously test them to ensure their validity and robustness in a variety of settings, temporal and spatial.

Northeastern Oregon has seen a dramatic shift in the management of its forests in the last few decades (Adams & Latta, 2003). Facing challenges such as increased presence of invasive pests and diseases, increased frequency and intensity of forest fires, changing harvesting regulations, and decreased infrastructure and capacity for timber processing, this once timber-dependent region has seen significant declines in harvesting (Adams & Latta, 2003). The magnitude of these declines, however, is highly dependent on land ownership class, be it public, private industrial or private non-industrial. Given the changing land management dynamics and resultant changing land cover (or *not* changing), this region serves as an excellent basis for remote sensing inquiry.

Accordingly, using a two-county area in northeastern Oregon as a basis for analysis, this study inquires into two of remote sensing's most valuable functions, single-time land cover mapping and land cover change mapping, all the while empirically testing a wide array of newly emerging and well-established methodologies. Additionally, a new method for change detection will be introduced and tested against other extant methods for accuracy. The results of this study are intended to at once inform local residents of the changes occurring in their landscape, provide the remote

sensing community with a robust assessment of a number of analytical techniques, and establish a repeatable general framework by which future land cover change studies can be performed.

Literature Review

This study is divided largely into two phases: (1) single-time land cover classification and (2) land cover change classification. A great number of steps are necessary to accomplish each of these phases and an even greater number of options exist in terms of remote sensing methods used to accomplish these goals. Accordingly, a wide variety of research was reviewed throughout the completion of this study to assist in making the informed decisions that are best suited for the specific project goals. In this section, a selection of critical works will be highlighted and their results discussed in relation to the project at hand. Each of the two phases will be discussed individually, broken down into their component parts and references will be made to the most relevant literature that guided the decisions made in this study.

Image Data

In the realm of remote sensing, one particular sensor has stood out amongst the rest as a uniquely flexible and extremely powerful basis for analytical inquiry -- Landsat. Among the lineage of sensors created by the broader Landsat program, Landsat 5 Thematic Mapper (TM) has proven particularly valuable, having contributed almost 30 years' worth of essentially uninterrupted data -- well beyond its expected life span of three years -- at a bi-monthly temporal resolution (Chander & Markham, 2003). This temporal

availability has made Landsat an invaluable resource for long-term land cover change analyses, such as the current project. A number of reviews have recently emerged in the remote sensing literature that highlight the importance of Landsat data in a broad array of disciplines (e.g. Green, 2006; Wulder *et al.*, 2008; Wulder *et al.*, 2012). The primary motivation for these studies stems from the uncertainty of the future of the Landsat program (Wulder *et al.*, 2008). After nearly three decades' worth of data collection and production, the Landsat program has finally reached a halt, with the most recent discontinuation of Landsat 5 TM in late 2011 and the scan line correction errors of Landsat 7 Enhanced Thematic Mapper Plus (ETM+). Green (2006) highlights the critical need for the continuation of the Landsat program, citing its unique spatial, spectral and temporal characteristics as a public good that should be governmentally-funded and made freely available to users. Wulder *et al.* (2012) presents data that document the significant increase in usage since the data was made freely available in 2008. In fact, from the time of initial free release, in October 2008, to September 2011 when the last Landsat 5 TM scenes were collected, there was a roughly five-fold increase in Landsat scene downloads per month. Despite an apparent data gap, the Landsat Data Continuity Mission (LDCM) is set to launch what will be deemed Landsat 8 in January of 2013 (Irons *et al.*, 2012). Irons *et al.* (2012) provide a description of the characteristics of Landsat 8, which will in many ways mimic the characteristics of the Landsat 7 ETM+ satellite in terms of spatial and spectral resolution, with the addition of two more shortwave infrared bands and an additional thermal band as well. Interestingly, Landsat 8 will be made available not only with geometric corrections already performed, but radiometric corrections as well -- a process that historically had to be done by the end-user. With the successful launch of

Landsat 8, users will once again be able to utilize Landsat's broad applicability to facilitate the study of a variety of earthly phenomena and ideally combine this new data with the wealth of historical Landsat data to enable future multi-temporal studies. While the methods used in this study apply specifically to Landsat 5 TM data, I believe that they could be easily extended to the newly acquired data of Landsat 8, further increasing the ability for long-term monitoring operations.

Image Pre-Processing

One of the critically important steps in a land cover change analysis is the ability to compare between images captured at different dates and times. Fortunately, with Landsat's temporal resolution, capturing the same image scenes every 15 days, this direct comparability is greatly facilitated. Unfortunately, however, it is rare that spatio-temporal conditions during each separate image capture will be precisely replicable from time to time, with sensor-specific calibration changes, and natural variations in atmospheric and solar illumination conditions (Rogan & Chen, 2004). Accordingly, three preliminary image pre-processing steps are necessary in order to maximize comparability between images: (1) radiometric correction, (2) atmospheric correction and (3) topographic normalization.

Radiometric and atmospheric correction are best considered as two parts of one whole process. Lu *et al.* (2002) highlight six primary reasons for performing radiometric and atmospheric correction, specific to Landsat 5 TM data: (1) within-scene multitemporal image analysis (e.g. land cover change), (2) across-path comparison of land cover types, (3) incorporation of and comparison between data from different

sensors (e.g. SPOT), (4) enhancing comparability to ground data (such as biomass estimations), (5) empirically-derived selected applications for using visible TM bands (such as aquatic plant bed mapping), and (6) accurate calculation of band ratios, such as vegetation indices. While only the first and last of this list are immediately pertinent to the current study, the wide applicability and necessary nature of radiometric and atmospheric correction should not be ignored. Broadly defined, radiometric correction is the process by which sensor-specific digital number (DN) values are converted to spectral reflectance values (Chander & Markham, 2003). While this may seem like a semantic difference, the DN values on a raw Landsat image, for example, are greatly affected by sensor-specific calibrations, such as gains and offsets (Chavez, 1996). A simple radiometric correction model, then, simply converts these DN values (typically unsigned 8-bit format, 0-255) to top-of-atmosphere (TOA) reflectance values (typically float single format, 0.0-1.0). Atmospheric correction, however, takes this process one step further by functionally removing the atmospheric effects (e.g. scattering) on this TOA reflectance, effectively resulting *ground* reflectance (Chavez, 1996). If done effectively, the spectral reflectance value of an object from an arm's length distance should mimic that seen on the corrected remotely sensed image. Naturally, a wide variety of methods have been proposed to accomplish this goal, largely divided into two categories (and two levels of complexity): empirical image-based methods (simpler) and those that require *in situ* atmospheric data (more complex).

A number of studies document the effectiveness of these methods (e.g., Moran *et al.*, 1992, Lu *et al.*, 2002). It is generally agreed that while incorporating *in situ* atmospheric measurements may increase the effectiveness of atmospheric correction,

simpler methods achieve comparable results in a much more cost-effective and time-efficient manner. One of the most common of the simpler, image-based techniques is known as cosine of the solar zenith angle, or COST, correction (Chavez, 1996). COST is a relative atmospheric correction technique based on the process of dark-object subtraction (DOS). According to Chavez (1988) the assumptions of a DOS model are (1) that there is a constant haze value throughout the entire image and (2) that there is a high probability that there are at least a few pixels on the imagery which should be "black" (0% reflectance) -- typically in shadows caused by topographic influence. Unlike more simple DOS models, however, COST incorporates the solar zenith angle into the equation, accounting for the effect of differential atmospheric transmittance (Chavez, 1996). With the study area's remoteness (no influence of urban smog), relatively high base elevations (*less* atmosphere to travel through), generally low humidity (little influence of atmospheric moisture), and significant topographic variability (ample presence of "black" shadows), the COST method's assumptions could be met and was accordingly selected as the atmospheric correction algorithm of choice.

Another critical variable that must be accounted for in multitemporal studies is the differential influence of topography on solar illumination. There are two primary solar variables that affect any given image: solar elevation (time of year) and solar azimuth (time of day). As the images used in this study were all collected at slightly different times, the effects from these factors cannot be assumed to be null. Particularly in mountainous regions (e.g., northeastern Oregon) a significant amount of spectral variability introduced by topographic slope and aspect is artificially induced, and should be corrected for (Civco, 1989). In medium resolution image datasets, such as Landsat,

northern-facing slopes (in the northern hemisphere) generally result in "darker" spectral responses, potentially introducing analytical difficulties into the digital remote sensing process, where misclassifications can result and image segmentations are also negatively affected (Civco, 1989). Meyer *et al.* (1993) described four specific topographic conditions particular to alpine environments, such as those in this study area, that can affect remote sensing analysis: (1) elevation dependency of optical thickness, (2) objects lying in the cast shadows of surrounding mountains, (3) well-illuminated slopes having a brightening effect on surrounding areas, and (4) the specific effect on irradiance of any given pixel is highly dependent on the sun-target geometry. While ideally one would like to account for all four of these conditions, topographic normalization efforts almost exclusively attempt to correct for the last of the four conditions, as the previous three are much more difficult to model accurately. There are generally two broad categories of topographic normalization: those based on the assumption of a Lambertian ground surface, and those based on the assumption of a non-Lambertian surface. The Lambertian model assumes that reflectance is independent of observation angle and that there is no diffuse illumination (Hantson & Chuvieco, 2011). The most common of the Lambertian correction methods is the simple cosine correction (Teillet *et al.*, 1982), which, although easily computed, is well-documented to over-estimate or over-compensate for the effects of illumination, effectively over-brightening the non-solar-facing slopes (Jensen, 2005). Two of the most common non-Lambertian techniques are Minnaert correction (Minnaert, 1941) and C-Correction (Teillet *et al.*, 1982). Both of these methods are empirical in nature, using the combined characteristics of the topography and band-specific reflectance to model the effects of differential illumination.

Minnaert requires *a priori* knowledge of the regional land cover, however, in order to get not only band-specific values, but also land cover-specific values. In many comparative studies (Meyer *et al.*, 1993; Riaño *et al.*, 2003; Hantson & Chuvieco, 2011), C-Correction has been shown to be the most effective topographic normalization method. Additionally, unlike Minnaert correction, no prior land cover classification was necessary for successful processing, facilitating the subsequent unbiased classification of the imagery based on project-specific needs

Radiometric/atmospheric correction and topographic normalization are not only intended to enhance comparability between images, but also to modify the imagery in such a way as to make it more representative of ground reflectance values. As a result, these steps enhance not only the change detection process, but also, importantly, the single-time land cover classification. To further enhance classification accuracy, it is common practice to perform a number of image transformations, band ratios and develop a variety of indices to capture information not readily gained in raw spectral data. Two of the most commonly used indices are the Normalized Difference Vegetation Index (NDVI) and the Tasseled Cap (TC) transformation.

Ratio datasets intended to highlight specific vegetation qualities not readily identifiable in raw imagery have been used since the 1960's (e.g. Jordan, 1969). A variety of simple ratios (SR) were used initially, typically involving some combination of the near infrared and red portions of the electromagnetic spectrum. The NDVI was introduced in the 1970s (largely credited to Tucker, 1979), which was a more complex ratio originally used on Landsat MSS data aimed at reducing the error associated with SR vegetation indices. Since its emergence in the field of remote sensing, NDVI and other

complex ratios have become widely accepted as powerful estimators of vegetation quantities, health, and densities (Rogan & Chen, 2004; Jensen, 2005).

The TC transformation was originally developed by Kauth and Thomas (1976) for the use in the realm of agricultural remote sensing on Landsat MSS data. Its original purpose was to be able to distinguish between agricultural crops across a broad geographic area over the life span of a crop, from soil, to healthy, growing crop, to late-season or "yellowing" crop, to harvesting (back to soil) - "Finally, the crop progresses back to the soil from whence it came (dust from dust?) by any of several routes" (Kauth & Thomas, 1976). The name, "Tasseled Cap" is derived from the shape of the x-y distribution that results that appears to take the shape "suggestive of a tasseled woolly cap" (Kauth & Thomas, 1976). In the original process, each of the four bands of Landsat MSS data was transformed linearly to produce four metrics that highlight these various stages and components of crop growth: (1) soil brightness, (2) "green stuff," (3) "yellow stuff," and (4) "non-such." It is a similar process to the Principal Components Analysis in that it transforms the data in order to capture a high percentage of the variability within the data in multi-dimensional, linear fashion. Crist and Cicone (1984) later adapted the four-band MSS TC transformation to the 6 reflective bands of the Landsat TM sensor shortly after the launch of Landsat 4 (further refined for Landsat 5 TM by Crist *et al.*, 1986). The three primary features that emerged from this modified transformation were (1) Brightness, intended, again, to highlight primarily soil qualities, (2) Greenness, highlighting healthy, growing vegetation, and (3) Wetness, a new product (in place of "yellow stuff"), which is intended to highlight both soil and vegetation moisture.

In addition to the agricultural realm, the TC has been utilized in a number of different land cover analyses, particularly in forested environments. Cohen *et al.* (1995), for example, explored the use of the TC transformation in estimating forest stand age and structure. They found that the Wetness index captured a significant amount of variability associated with tree species-based stand type. Similarly, Wulder *et al.* (2004) documented TC Wetness' effectiveness in predicting forest stand age after harvesting using Landsat 7 ETM+ imagery. In addition to single-time land cover classification, Healey *et al.* (2005) explored the use of the TC transformation in detecting forest cover change. In that study, a linear transformation of all three TC features (deemed the Disturbance Index) was found to be an excellent estimator of forest harvesting activity.

Lastly, in order to further enhance classification, particularly in areas where regional topography is closely linked with land cover as is often the case, a number of studies have advocated the use of ancillary topographic data to increase accuracies. Rogan *et al.* (2003) incorporated elevation, slope and aspect into their classification and regression tree-based classification model and found that ancillary data accounted for an approximately 15% increase in overall classification accuracy. Similarly, Treitz and Howarth (2000) found that using elevation data increased the ability to discriminate between different forest ecosystem types.

Segmentation Parameter Analysis and Land Cover Classification

Landsat 5 TM imagery, given its longevity, has lent itself well to a wide variety of methodological approaches. Until relatively recently, the vast majority of analytical endeavors performed on Landsat imagery (and any other image types) took place on a

pixel-by-pixel basis. That is, each individual picture element (pixel, raster, grid cell) was treated relatively independent of one another in the classification process. More recently, however, with the emergence of many higher resolution imagery sources (such as IKONOS, QuickBird, and WorldView), the unique value of individual pixels on any given image has decreased, leading to the proliferation of object-based image analysis (Blaschke, 2011). Object-based image analysis (OBIA) is built upon the process of image segmentation, where images are divided into pixel groupings that share similar characteristics, both spectrally and spatially. Blaschke (2010) provides an excellent review of the current state of OBIA throughout the remote sensing literature. In it, he highlights a number of landmark occurrences that have led to a proliferation of the quantity and complexity of OBIA research emerging from the remote sensing community.

As stated above, however, a common thread throughout the research is the tendency for the use of OBIA on high resolution imagery. Accordingly, relatively little research has been done on the efficacy of using OBIA methods on coarser resolution datasets such as Landsat 5 TM. Conceptually, one can imagine that the utility of OBIA in studying Landsat data depends on the scale of analysis. For example, if OBIA improves the classification accuracy of a 1:10,000 scale analysis with 3 m resolution imagery, then potentially it could be similarly valuable for a 1:100,000 scale analysis with 30 m pixels. There is uncertainty, however, in the literature as to the effectiveness of OBIA with Landsat. For example, Dorren *et al.* (2003) compared Landsat OBIA to pixel-based methods in mapping forest stand types across a relatively small area (530 m²) with very mountainous terrain. It was found that pixel-based outperformed object-based

methods. That said, despite the lower accuracies, the authors suggest that the stand type results were potentially more "useful" (less so-called "salt and pepper effect"), and could function as more appropriate management units. Additionally they highlighted a number of factors that could improve OBIA studies with Landsat data, including improved accuracy assessment methods and a more insightful segmentation process (both discussed later). Jobin *et al.* (2008) provided a lukewarm account of OBIA, suggesting it *may* improve Landsat-based habitat mapping based on their results, but without a comparison to pixel-based methods, this suggestion should only be taken anecdotally. A few studies have, however, found OBIA to result in at least comparable and in some cases higher accuracies using Landsat data. Myint *et al.* (2008), for example, documented OBIA's effectiveness in mapping the change damage that resulted from a tornado in Oklahoma, finding its results to be significantly improved over traditional methods. Similarly, when performing a landscape-level forest fragmentation study, Newman *et al.* (2011) found OBIA methods to greatly improve classification accuracy, given the ease of including ancillary data to aid in the classification process. In addition, Newman *et al.* (2011) found that OBIA forest fragmentation results were significantly different than similar metrics computed in a pixel-based environment. This makes sense, given the fact that resultant image objects will be much more compact and spectrally homogeneous than the typically more variable pixels. Geneletti and Gorte (2003) propose an OBIA technique that incorporated the use of higher resolution aerial photography with Landsat in order to obtain higher classification accuracies -- in some ways comparable to a pan-sharpening technique.

In general, based on the sparse results of these few studies, there appears to be no overall agreement as to whether or not OBIA improves classification accuracy over pixel-based analysis for Landsat data. Although there is perhaps a slight tendency for better results (or at least improved utility of the results), the paucity of coarse resolution OBIA studies warrants a significant amount of further research before any sound conclusions can be drawn. Additionally, throughout all of the aforementioned OBIA-related papers, there is a common emphasis on the importance of the segmentation process on the resultant classification. A number of studies exist that inquire specifically into the process of segmentation and the effect on classification results. Rasi *et al.* (2011), for example, used multi-date Landsat imagery for change detection and classification and in doing so explored the segment sizes that result from changing segmentation parameters. Anders *et al.* (2011) found that in mapping geomorphological features, each separate feature category (glacial, fluvial, karst, etc.) required different input segmentation parameters to perform optimally.

It is appropriate here to discuss what is precisely meant by "segmentation parameters." The foremost software package used throughout the vast majority of OBIA studies has been Trimble eCognition (formerly Definiens eCognition). eCognition's unique multiresolution segmentation algorithm combines three levels of segmentation characteristics into the process, as shown in Figure 1 below.

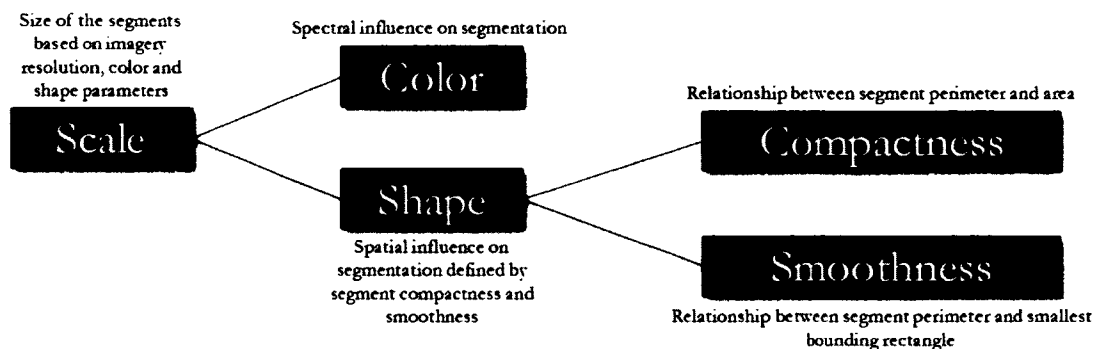


Figure 1. eCognition's multiresolution segmentation parameters (Batz and Schäpe, 2000)

Batz and Schäpe (2000) provide the best description of these parameters and the process that results. Multiresolution segmentation is a bottom-up segmentation approach -- that is, it begins at the pixel levels and grows segments simultaneously throughout the image based on local homogeneity criteria. When this region growing stops is dictated by the scale parameter, or, as Batz and Schäpe (2000) describe it, a "degree of fitting" parameter. With a small scale parameter, there will be many small segments; with a large scale parameter, there will be fewer larger segments. The scale parameter is further refined by the designation of color and shape parameter inputs, or spectral and spatial homogeneity. If full influence is given to color, the segments are grown purely with regards to the image spectral characteristics, completely ignoring object shape. The color parameter is generally defined as the weighted sum of the spectral standard deviations per spectral band within a given object (Batz & Schäpe, 2000). The shape parameter is not a measure in and of itself, but rather a combination of two additional parameters, compactness and smoothness. Compactness, quite simply, is the ratio between the length of the object perimeter and the square-root of its area (Batz & Schäpe, 2000). Smoothness, which is closely related, is the ratio between the length of the object

perimeter and that of the smallest bounding rectangle (Baatz & Schäpe, 2000). Taken together, these variables represent spatial homogeneity. If full influence (or 90% influence, as is limited by eCognition software) is given to the shape parameter in the segmentation process, the resultant objects would be very compact, near circular or square shapes, almost completely ignoring the spectral characteristics of the imagery.

Up until relatively recently, a typical methodology for segmentation parameter selection was a simple visual, qualitative assessment of the resultant segments (i.e., "Do these segments visually match what is happening on the ground?"). Of particular interest in the segmentation literature in recent years, however, is finding more objective, automated ways to determine these optimal segmentation parameters. Espindola *et al.* (2006) proposed a spatial autocorrelation-based region growing segmentation algorithm that at once maximizes within-segment spectral homogeneity and between segment heterogeneity. Similarly, Gao *et al.* (2011) explored the use of the Separability and Thresholds (SEaTH) algorithm for segmentation parameter selection and found it to produce classification accuracies higher than traditional parameter selection and classification methods. Moller *et al.* (2007) inquired into the process of assessing the accuracy not of the resultant OBIA classification, but of the segment boundaries themselves, introducing the so-called "Comparison Index," which measures topological agreement between ground features and image segments (i.e., "Do these segments *quantitatively* match what is happening on the ground?). Despite various attempts to model the optimal segmentation parameters, no general agreement has been reached. As suggested by Anders *et al.* (2011) and others, the success of segmentation is highly dependent on image- and scene-specific characteristics. Accordingly, simpler empirical

methods are believed to be best-suited for a segmentation parameter analysis. Using empirical, trial-and-error-based methods, it is believed that optimal segmentation parameters can be determined in a highly objective fashion, across broad range of study areas.

With the release of eCognition 8.7 (2011), four new classification algorithms were implemented into the software. These four can be divided into parametric (Bayes) and non-parametric classifiers (decision tree, support vector machine, and k -nearest neighbor) (Trimble, 2012). Given the proprietary nature of eCognition software, information about the specifics of the classification algorithms is notably sparse. Accordingly, these descriptions (gleaned largely from the Trimble eCognition Community, 2012) should be treated as generalizations about their broader principles, rather than software-specific implementation. Bayes is a probabilistic classifier based on Bayes' theorem that assumes strong independence of the input variables (although it has been shown to perform well even when this assumption is not met -- see full discussion in CONCLUSIONS). Relatively few studies have explored the utility of Bayes-based classification in the remote sensing literature (e.g., Lau & Hsiao, 2005; Pradhan *et al.*, 2010). There is a particular paucity with regards to object-based methods, where non-parametric methods appear to take precedent. Those that have explored Bayes in remote sensing, however, indeed demonstrate its utility as an effective classification tool.

The decision tree classification method (more commonly known as classification and regression trees (CART)), was first introduced by Breimann *et al.* (1984). CART is a non-parametric data mining tool that recursively splits the data into a series of increasingly homogeneous end nodes that are able to predict the dependent variable

(Rogan *et al.*, 2003). Unlike Bayes, CART makes no assumptions about the input data and can operate on both continuous and categorical data types. As such, CART has received a lot of attention in the remote sensing literature in recent years, especially in conjunction with the proliferation of object-based image analysis methods, because of its ability to incorporate a wide variety of input data and parameter estimates in the classification process. Additionally, unlike complex methods like support vector machines and artificial neural networks, the CART classification process yields a visual account of the actual tree after classification has been performed, so the user can see what input data was most valuable in the classification process and also see where it may have gone awry (Borak & Strahler, 1999). As mentioned previously, Rogan *et al.* (2003) explored the utility of CART in a classification model that facilitated the incorporation of not only a variety of different spectral data, but also ancillary data such as elevation, slope and aspect. In being able to include these extra variables into the decision tree, resultant image classification accuracies were significantly improved.

Support vector machine (SVM) and k -nearest neighbor (KNN) classification algorithms, although both valuable in their own right were not explored in this study and as such will not be discussed in great detail. Broadly speaking, however, SVM is a complex machine learning tool that transforms input data in n -dimensional feature space, attempting to group similar data together and form hyperplanes, or dividing lines, between different outcome variables. KNN, on the other hand, is a much simpler machine learning tool whereby unknown data points are simply classified by the majority of a predetermined number (k) of nearby training data in n -dimensional feature space.

Accuracy Assessment

Accuracy assessment is one of the most critical steps in any remote sensing analysis. Since its emergence in the field of remote sensing in the early 1980s, thematic accuracy assessment has become an integral component in the digital image analysis process, often serving as the base measure of success in land cover classifications. The error matrix is the primary tool by which this accuracy assessment occurs (Congalton & Green, 2009). In an error matrix, reference data (usually collected through ground sampling and/or photo interpretation) aimed at representing the actual ground conditions are compared to the results of a thematic land cover classification (Congalton & Green, 2009). From this matrix, a number of accuracy estimates can be gained; namely class-specific user's and producer's accuracies, overall accuracies (Story & Congalton, 1986), and a number of more complex statistics, including the well-established Kappa, or Khat, statistic (Congalton *et al.*, 1983). User's accuracies estimate the degree to which a user of the resultant classification map will be able to reliably use the classification of any given land cover classification for his or her analysis. Producer's accuracies estimate the degree to which the map producer was able to accurately classify the imagery based on the sample data. Overall accuracy uses the matrix's major diagonal (correctly classified samples) and compares that number to the total number of samples used in order to estimate accuracy of the entire classification. Kappa, originally adapted from Cohen (1960) is a multivariate, statistical measure of accuracy that incorporates all of the data contained within the matrix, normalizing the overall accuracy to include the element of chance agreement and as a result facilitates the comparison between different error matrices.

Reference data sample selection is a critical component to the assurance of a representative accuracy assessment. Using Landsat 5 TM imagery in a pixel-based environment, the widely accepted guidelines state that, in order to minimize the spatial and thematic error associated with field collection methods (i.e., GPS inaccuracy) and image characteristics (i.e. positional inaccuracy), a sample area of at least 3 x 3 pixels should be used (Congalton & Green, 2009). Additionally, in order to get a representative sample, a rule of thumb is that at least 100 samples per class should be taken (divided into training and accuracy assessment data) (Congalton & Green, 2009). Lastly, these samples should be well-distributed across the entire study area, to avoid sample spatial autocorrelation and to represent land cover types across what may amount to be a wide range of ground conditions, depending on the size of the study area (Congalton & Green, 2009).

In the traditional error matrix, these samples are treated as individual units and resultantly are given equal weight in the accuracy assessment process. This makes perfect sense in a pixel-based environment, where the ground sample units are assumed to have the same spatial extent (e.g., 3 x 3 pixels). In an object-based environment, however, where the image objects (and reference samples) can vary significantly in size, perhaps these samples should be assessed not only in terms of their totals, but weighted by the object spatial extent as well. Radoux *et al.* (2011) suggested this area-based weighting should be included in the accuracy assessment process. MacLean and Congalton (2012) applied this area-weighting scheme to the traditional error matrix, facilitating the computation of the aforementioned accuracy estimates (user's, producer's, overall, and Kappa accuracies). To date, little research has been done on the comparison

between the traditional error matrix and the area-based error matrix. This study will contribute some of the first work done on such a comparison, looking at the resultant accuracies between the two methods and suggesting mechanisms that might explain the results.

Land Cover Change

Remote sensing has been widely used in the fields of natural resource management and ecology, particularly in regards to long-term and broad-scale monitoring operations. Cohen and Goward (2004) and Roughgarden *et al.* (1991) provide an excellent account of this usage, documenting a number of examples of practical and effective uses of remote sensing technologies throughout the ecological discipline. This wide range of applications includes, but is certainly not limited to, thematic land cover classification, approximation of floral biophysical properties, characterization of phenological and disturbance-related vegetation changes, monitoring of the urban-wildland interface, and the unique ability to assess ecological activity across vast tracts of land and long spans of time, standing in stark contrast to the more typical field-based monitoring methods dominant in ecology and natural resource management.

Of particular interest to this study is research that relates to land use and land cover changes over time. Rogan and Chen (2004) and Treitz and Rogan (2004) provide comprehensive review of the various considerations that go into a land cover change analyses, from selecting the optimal imagery type, to image pre-processing, change detection, and finally change classification. At each one of these steps, there are a number of decision points to be carefully vetted and, in accordance with project-specific

goals and research questions, selected by the remote sensing scientist. As the first two steps have already been discussed, the final portion of this review will discuss methods for change detection, change classification techniques, and change detection accuracy assessment.

A variety of methods exist for the detection of land cover change on digital imagery. Coppin *et al.* (2004) and Lu *et al.* (2004) all provide excellent reviews summarizing progress throughout the remote sensing discipline in the development of change detection methods, highlighting the most widely used techniques and citing literature-based examples that employ their usage. Change detection analyses fall largely into one of two categories: (1) post-comparison of separately classified images at two (or more) different dates and (2) simultaneous analysis of multitemporal data. The first method is widely used for its relative ease of comprehension and a lack of necessity to radiometrically correct the images, but also suffers from a few fatal flaws. Namely, unless entirely photo-interpreted, gathering reference data at a variety of temporal intervals is difficult (and, unless prior work has been done, impossible), and errors in each individual classification are compounded in the post comparison method. Accordingly, these methods are not as frequently practiced throughout the discipline. The latter category (simultaneous multitemporal image analysis) contains a wide variety of options (according to Coppin *et al.*, 2010): (1) composite analysis; (2) univariate image differencing; (3) image ratioing; (4) bi-temporal linear data transformation; (5) change vector analysis; (6) image regression; (6) multitemporal spectral mixture analysis; (7) multidimensional temporal feature space analysis; and (8) experimental and hybrid

algorithms. Lu *et al.* (2004) developed a similar categorization of change detection methods, but incorporated GIS-based methods and simple visual interpretation methods.

While a specific explanation of each of these change detection algorithms is beyond the scope of this literature review, a justification of the univariate image differencing method used in this study is warranted. First and foremost, this process is recommended by the well-established National Oceanic and Atmospheric Administration's (NOAA) Coastal Change Analysis Program (C-CAP). This program has developed a comprehensive guide for regional implementation of land cover change analyses (Dobson *et al.*, 1995), whose recommendations for land cover change analysis methods were closely followed in this study. In it, Dobson *et al.* (1995) suggest the following protocol: (1) a classification is performed on the most recent scene (Y2); (2) a univariate image differencing is performed between Y2 and Y1; (3) a threshold for change is established (per class); and (4) only those areas masked as change are classified for Y1. Xian *et al.* (2009) described a similar process used to update the 2001 National Land Cover Database (NLCD) to 2006.

In addition to its usage in two widely used datasets (C-CAP and NLCD), univariate image differencing is the most widely applied and easily interpretable change detection algorithm (Coppin *et al.*, 2004). Additionally, Lu *et al.* (2004) suggest that in looking for binary land cover changes (such as forest to non-forest and vice versa) that image differencing is the most preferable. Methodologically speaking, image differencing involves the single-band differencing (or subtraction) of a given digital image from another precisely registered (and ideally, radiometrically corrected) image at a different date. Under ideal conditions, the resulting difference image would have a

roughly normal frequency distribution about the mean of 0 (which can be assumed to be "non-change" areas). Beyond a certain threshold in each direction, however, it is assumed that change has occurred. Studies have used a wide variety of bands in these univariate differencing analyses, and it is very common to use not only raw spectral bands but derivative information (i.e., NDVI, TC) as well. Wilson and Sader (2002), for example, explored the use of the NDVI and normalized difference moisture index (NDMI) to detect forest cover changes due to harvesting and found that the NDMI outperformed the NDVI in detecting change. Mas (1999) however, found TM band 2 to perform comparably well to NDVI. Healey *et al.* (2005) used the TC transformation to detect forest cover changes and found that a linear combination of all three features was the best at identifying forest disturbance events. Ridd and Liu (1998) found that, in using all six spectral Landsat TM bands and the three main TC features (brightness, greenness, wetness), that each performed well in its own right with regard to specific land cover from-to change types. Clearly, little generalized agreement has been reached as to which spectral or derivative bands are preferable for change detection. Accordingly, it is believed that specific image differencing bands should be chosen empirically according to the regional land cover characteristics and the desired land cover change information.

An important element of single band or univariate image differencing is the determination of thresholds by which the data distribution can be density sliced into change and non-change classifications. These are typically represented as standard deviations from the mean value (which, again, should ideally be 0) (Fung & LeDrew, 1988). Importantly, as suggested by Xian *et al.* (2009), not all land cover classes experience the same degree of change. Cropland, for example, experiences greater

changes spectrally in a single season than perhaps unharvested forest land would experience in a decade. Accordingly, it is important to determine class-specific change-no change thresholds. There are a number of ways to determine the optimal change thresholds, but Fung and LeDrew (1988) suggest a simple empirical testing and accuracy assessment comparison, as is done in this study.

Objectives

Therefore, the objectives in this study can be divided into two broad categories: methods and applications. The latter can be seen as the motivation for the former. They are as follows:

1. To accurately quantify the spatial distribution of land cover types across the entire study area in 2011, and in doing so:
 - a. Test the process of image segmentation using a variety of input parameters;
 - b. Compare the classification accuracies of object-based and pixel-based analyses;
 - c. Compare the classification accuracies of parametric and non-parametric classifiers;
and
 - d. Explore the use of an area-based error matrix for accuracy assessment.
2. To accurately quantify the spatial distribution of land cover changes that have occurred across the study area from 1986 to 2011, and in doing so:

- a. Introduce a new principal component analysis-based change detection technique;
- b. Test this technique against 10 other spectral and derivative change detection bands;
- c. Determine optimal change thresholds;
and
- d. Quantify forest harvesting and regeneration across different land ownership classes.

CHAPTER II

METHODS

Study Area

The study area encompasses much of Union and Baker Counties in northeastern Oregon, USA (Figure 2). The combined area of these large, sparsely populated counties is 13,270 km², more than half the size of the State of New Hampshire. According to the 2000 US Census, they possessed a combined population of 41,882 resulting in a density of just above 3 persons/km², while the population density for Oregon was about 15 persons/km² (Union and Baker counties included). Coupled with this overall sparseness is the fact that almost three-quarters of the area's population (72%) lives within Census-designated "places," which are more densely-developed town and city centers. This study area contains vast tracts of uninhabited land, much of which is owned by the Federal Government. In fact, in these two counties, 6,699 km² (51%) of the land is under public ownership, managed primarily between the United States Forest Service (5,111 km², 76%) and the Bureau of Land Management (1,487 km², 22%). A complete account of ownership totals and percentages can be seen in Appendix 1.

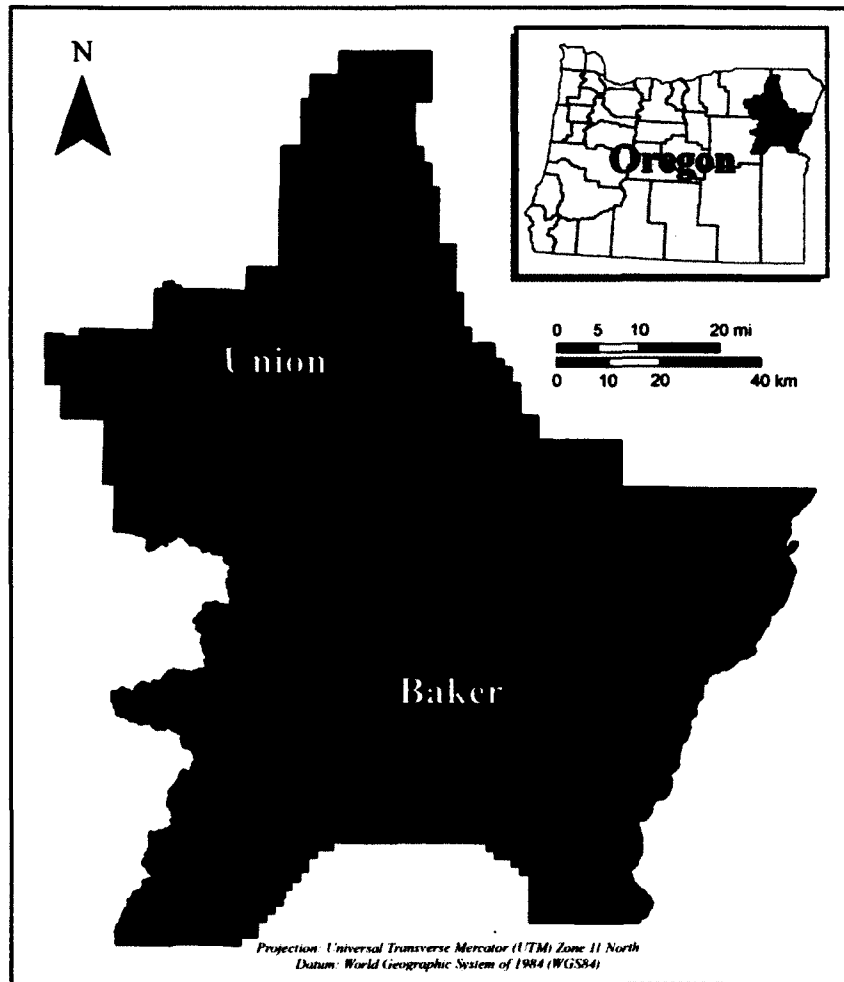


Figure 2. Study area map, Union and Baker Counties, Oregon

The region is characterized by a highly varied topography ranging from very mountainous terrain to expansive valley bottoms. Elevations range from 512 m at the lowest point to 2915 m atop the area's highest peak, Eagle Cap Mountain. With an overall average elevation of 1321 m, over half of the landmass (56%) lies between the elevations of 1000 and 1500 m. There are two predominant mountain ranges that bound the study area to the east and west. The Wallowa Mountains form much of the eastern boundary of the study area, while the Blue Mountains lie to the west. Depending on the

scale being considered, these ranges are typically considered entirely separate geologic regions, but they are often grouped into the greater Blue Mountain region of the interior northwestern United States.

Given the highly varied terrain, there are stark contrasts between different land cover types that dominate this area. Located on “the dry side” of the Cascade Mountains, this region gets relatively little precipitation (a total of 44 cm recorded at KLGD weather station, the area’s largest airport, from January 1 to December 31, 2011). Large water bodies are relatively few and far between, with only a few notably-sized lakes and rivers being present throughout the two-county area. As a result, forested environments are found primarily in the mountains, where temperatures remain consistently cool enough and sufficient moisture is retained to enable tree growth. Despite this relative aridity, cropland is plentiful on the valley bottoms, benefitting from heavy irrigation and fertile Mount Mazama ash soils. In between these two extremes, there is a dominance of two land cover types: grassland and shrub/scrub. The former tends to fill the elevation transition zone between cropland and forest and is often found in drier patches and south-facing slopes within the forested areas. The latter dominates the middle elevations of the southern portion of the study area, forming vast expanses of rolling hills dominated by sagebrush with little to no undergrowth.

For the purposes of this study, elevations above 2000 m and designated wilderness areas were removed from consideration. It is believed that land cover changes that occur in these areas are simply the result of differential presence/absence of snow and/or other natural disturbance events (e.g. fire). Of interest to this study are only the anthropogenic effects on regional land cover.

Reference data

A six-class land cover classification scheme was used for this study, both in terms of single-time land cover classification and land cover change analysis. The definition of these classes was determined based on expert knowledge of regional landscape dynamics, an inquiry into existing land cover datasets (such as the 2006 National Land Cover Dataset (NLCD)), visual examination of a variety of imagery types (such as Landsat and NAIP data), and a series of unsupervised classifications. This broad classification was also created with the project-specific mindset of being able to accurately classify forest-related land cover changes in the region. The specific class definitions are described as follows:

Cropland	Irrigated and/or cultivated vegetation characterized by a high degree of seasonal influence
Developed	Any anthropogenic land development or non-vegetated disturbed landscape including bare ground
Forest	Areas with greater than or equal to approximately 20% canopy closure of naturally occurring, primarily coniferous trees
Grassland	Non-irrigated, non-cultivated herbaceous vegetation
Shrub/Scrub	Sagebrush or other shrubland with a barren or grassy underlying ground cover
Water	Rivers, streams, lakes, ponds, reservoirs, and submerged wetlands

Ground-based land cover reference data were collected between the months of June and August in 2011. Global positioning system (GPS) data were captured using a Trimble YUMA tablet GPS unit equipped with ESRI ArcPad 10 software. Sample data collection was performed on an opportunistic basis, with land cover reference sample units being selected based upon a number of criteria. These criteria are as follows: (1) the unit area must be at least 3,600 m² in size (3 x 3 Landsat 5 TM pixels); (2) the land cover must be visually (and spectrally) homogeneous within the entire sample unit; (3) the collective samples of a given land cover class must capture a high degree of variability in order to ultimately classify the land cover accurately despite *within class* spectral and spatial variation; and (4) every attempt must be made to spatially distribute these sample units across the entire study area to avoid sample spatial autocorrelation and get a good distribution of samples. To aid in the process of satisfying criterion 2 above, an unsupervised classification was performed on a 2010 Landsat 5 TM scene and loaded into the GPS unit for *in situ* visual inspection of spectral homogeneity. Criterion 4 was relatively difficult to satisfy in many cases, given the sparseness of road network coverage in this rural region and given the restrictions imposed by avoiding trespassing on private lands. In many cases, as a result, GPS coordinates were taken with an offshoot distance and azimuth from the roadside. Subsequent to field data collection, these sample units were carefully edited through photo interpretation of high- and medium-spatial resolution imagery (2011 National Agricultural Inventory Program (NAIP) and Landsat 5 TM data, respectively) to ensure accuracy of spatial location and thematic labeling. Sample units were adjusted, removed, and/or added as necessary.

The classes and their accordant sampling totals can be seen in Table 1. These totals reflect an initial goal of collecting 100 samples with a minimum mapping unit of 3,600 m² for each land cover class to enable accurate classification model training and to ensure statistical validity in accuracy assessment (Congalton & Green, 2009). In order to avoid high sample spatial autocorrelation and to minimize spectral redundancy in land cover classes that were fairly sparsely distributed or were found in units of insufficient size, these totals were altered for the classes of Water and Developed. The reference samples were then randomly divided into two groups; data used to train the classification model and data used to assess the thematic accuracy of the classification.

Cropland	100	50	50
Developed	80	40	40
Forest	100	50	50
Grassland	100	50	50
Shrub/scrub	100	50	50
Water	60	30	30

Table 1. Land cover reference data

Image Data

Landsat 5 Thematic Mapper (TM) data was the primary image type used in this study. All images were obtained from the United States Geological Survey's (USGS) Global Visualization Viewer (GloVis, <http://glovis.usgs.gov/>) in GeoTIFF format. Two Landsat 5 TM scenes were needed to encompass the vast majority of Union and Baker counties: (1) Path 43, Row 28 (approximate scene center: 46°1'50.9"N, 117°46'19.2"W) and Path 43, Row 29 (44°36'43.9"N, 118°17'9.6"W). Fortunately, these two scenes fall within the same orbital path, meaning their image capture was part of a continuous data

collection swath. This results in a seamless mosaic between the two scenes, both spatially and spectrally. A small portion of the southeastern corner of Baker County was cut off from this Landsat path, and accordingly was removed from the study area (see Study Area). Given the insignificant size of the area removed, it was believed that the costs of omitting this fairly non-forested, unpopulated area outweighed the benefits of avoiding incorporating an entirely different scene from a Landsat path 42 (and resultantly, a different date of image capture).

A temporal series of late spring to early fall images (May-October) were obtained at a 5-year interval between the years of 1986 and 2011. Only those images with very low cloud cover (<5%) were deemed acceptable for this study. In order to capture the seasonality of the highly moisture- and temperature-dependent land cover classes in this region, two images were used for each year of interest. An "early summer," or growing season image and a "late summer," or senescence image were used in the classification process. As the late summer images ultimately played a more significant role in the classification process, every effort was made to utilize near-anniversary images at or around the end of August into early September. The exception to this rule was the year of 1986, during which the cloud-free, senescence image availability was limited to October. The time frames of the early summer images were more variable, given the typically higher cloud cover present during the growing season. The resultant image dates can be seen in Table 2.

2011	07/09	08/26
2006	06/25	08/28
2001	05/10	08/30
1996	06/13	09/01
1991	07/02	09/04
1986	07/20	10/08

Table 2. Landsat 5 TM image dates

Image Pre-Processing

All images used in this study were pre-processed using ERDAS Imagine 2011 software. To enhance comparability between images and to aid in the classification process, each image underwent the same series of pre-processing steps. These steps proceeded as follows: (1) image stacking, (2) image mosaicking, (3) clipping to study area spatial extent, (4) geometric registration, (5) atmospheric correction, (6) topographic normalization, (7) derivative and ratio band generation, and (8) band rescaling. Each of these steps is described in detail below. A model was built using ERDAS Model Maker that incorporated a number of these steps to facilitate processing efficiency and to ensure data consistency.

Each image downloaded in raw format from USGS GloVis came with seven separate GeoTIFF files, each representing a different spectral band of a Landsat 5 TM scene. Accordingly, the first necessary step involved stacking these images together into a single, unsigned 8-bit (0-255) ERDAS Imagine image file (*.img format). As band 6 (thermal) was of a different spatial resolution than the other six bands (120 m vs. 30 m, respectively), it was excluded from the image stack. For each year of interest, the two Landsat scenes (Path 43, Row 28 and Path 43 Row 29) were mosaicked together using “maximum” as the overlap function, in order to minimize the presence of image seams.

To reduce file size and further increase processing efficiency, these mosaicked images were clipped to the spatial extent of the study area. During the clipping process, the images were geometrically registered to one another so that their pixels would precisely overlay one another. A nearest neighbor re-sampling algorithm was used to maintain the spectral integrity of the original data (Jensen, 2005).

In order to enhance comparability between images taken at different dates, times and atmospheric conditions, two image pre-processing techniques were employed: (1) atmospheric correction and (2) topographic normalization.

All images were processed using the image-based relative atmospheric correction method known as COST correction (Chavez, 1996). The COST corrected surface is calculated as follows:

$$\rho = \frac{\left[\pi d^2 \left(L_{min} + \frac{DN_i(L_{max} - L_{min})}{DN_{max}} \right) - \left(L_{min} + \frac{DN_{min}(L_{max} - L_{min})}{DN_{max}} \right) - \left(\frac{0.01d^2 \cos^2 \theta_z}{\pi E_{sun}} \right) \right]}{E_{sun} \cos^2 \theta_z}$$

Where d is the sun-earth distance, L_{min} and L_{max} are spectral radiance calibration factors, DN_i is the DN value at a given pixel i , DN_{max} is the maximum possible DN value (255 for 8-bit data), DN_{min} is the band-specific minimum DN value found through an exploration of the layer histogram (smallest value with ≥ 1000 pixels), and E_{sun} is the solar spectral irradiance. L_{min} , L_{max} , E_{sun} , and d can all be found in Chander & Markham (2003). It is important to note that the resulting imagery converted unsigned 8-bit DN values to 32-bit float single reflectance values (0-1). For the purpose of maintaining the high level of precision enabled by such a format, all of the subsequent

image pre-processing was performed using a float single format. Ultimately, however, these data were converted back to unsigned 8-bit to reduce data storage and increase processing efficiency.

Each image was then topographically normalized using the C-Correction method (Teillet *et al.*, 1982). The first step in the C-Correction process is to determine the magnitude of illumination across the entire study area, as defined by:

$$Illumination = \cos \gamma_i = \cos \theta_z \cos \alpha_s + \sin \theta_z \sin \alpha_s \cos(\delta_a - \delta_o)$$

Where γ_i is the solar incidence angle relative to the sloped ground surface, θ_z is the solar zenith angle, α_s is the slope of the ground surface, δ_a is the solar azimuth angle and δ_o is the aspect of the ground slope. In order to create an illumination surface, a USGS 30-m Digital Elevation Model (DEM) was used. Slope and aspect surfaces were generated using the ArcMap 10 Spatial Analyst extension, resampled using cubic convolution and geometrically registered to the Landsat imagery. For each image date, the solar zenith angle (inverse of solar elevation) and azimuth were obtained from each of the Landsat scenes' header files and averaged for the mosaicked image. Again, because these two scenes were captured as part of a continuous swath, the differences between solar elevations and azimuths were negligible. The resultant illumination surface was stacked with the six-band Landsat image and a per-pixel least squares linear regression was run to determine the relative effect of illumination on the "brightness" of the pixel in each spectral band. The purpose of this empirical adjustment approach is to normalize the data such that the presumed positive relationship between illumination and DN value

would be reduced to a null effect. In order to do so, the C-Correction (Teillet *et al.*, 1982) algorithm was used:

$$DN_{\lambda i, h} = DN_{\lambda i} \left(\frac{\cos \theta_z + c_\lambda}{\cos \gamma_i + c_\lambda} \right)$$

Where $DN_{\lambda i, h}$ is the DN value of a pixel (i) in a given spectral band (λ) on a horizontal surface (h) (with no influence of solar illumination), $DN_{\lambda i}$ is the value of that pixel on a sloped surface (subject to illumination influence), and c_λ is a band-specific parameter defined by slope (m_λ) and y-intercept (b_λ) of the linear regression line between illumination and DN values such that:

$$c_\lambda = \frac{b_\lambda}{m_\lambda}$$

With each image corrected in such a way as to best represent its true on-the-ground spectral conditions, a number of derivative bands were generated to enhance the accuracy of the subsequent image classification and analysis. The NDVI for Landsat 5 TM data was calculated as such:

$$NDVI = \frac{(band\ 4 - band\ 3)}{(band\ 4 + band\ 3)}$$

Additionally, the first three TC transformation features (Brightness, Greenness, and Wetness) were generated. The multiplicative linear transformation values, as modified for Landsat 5 TM data by Crist *et al.* (1986) can be seen in Table 3.

Feature	Landsat TM band					
	1	2	3	4	5	7
Brightness	0.2909	0.2493	0.4806	0.5568	0.4438	0.1706
Greenness	-0.2728	-0.2174	-0.5508	0.7221	0.0733	-0.1648
Wetness	0.1446	0.1761	0.3322	0.3396	-0.6210	-0.4186

Table 3. Tasseled Cap transformation for Landsat 5 TM

With all of the derivative information created, the data were then able to be combined for each image date into a 10-band image (6 raw spectral bands, 1 NDVI, 3 TC). In order to do so, the 6-band atmospherically- and topographically-corrected Landsat image was first rescaled from float single format to unsigned 8-bit. The radiometric dynamic range for each of the images was then computed through an examination of the image histograms. For the purpose of this study, the dynamic range was determined to be the range of DN values with frequencies greater than or equal to 1,000 pixels. The four derivative layers for each image date were then rescaled to the image dynamic range of its corresponding 6-band image in order to be comparable to the original raw imagery. The 10 resulting 8-bit bands were then stacked together into a single image. For each year of interest, the early and late summer 10-band images were then stacked together to form a 20-band image. Finally, given the important link between land cover and topography in this region, slope, aspect and elevation layers were rescaled to unsigned 8-bit as well, stretched to the dynamic range of the late summer image.

These three topographic datasets were then stacked with the 20-band image to create a 23-band image as seen in Figure 3.

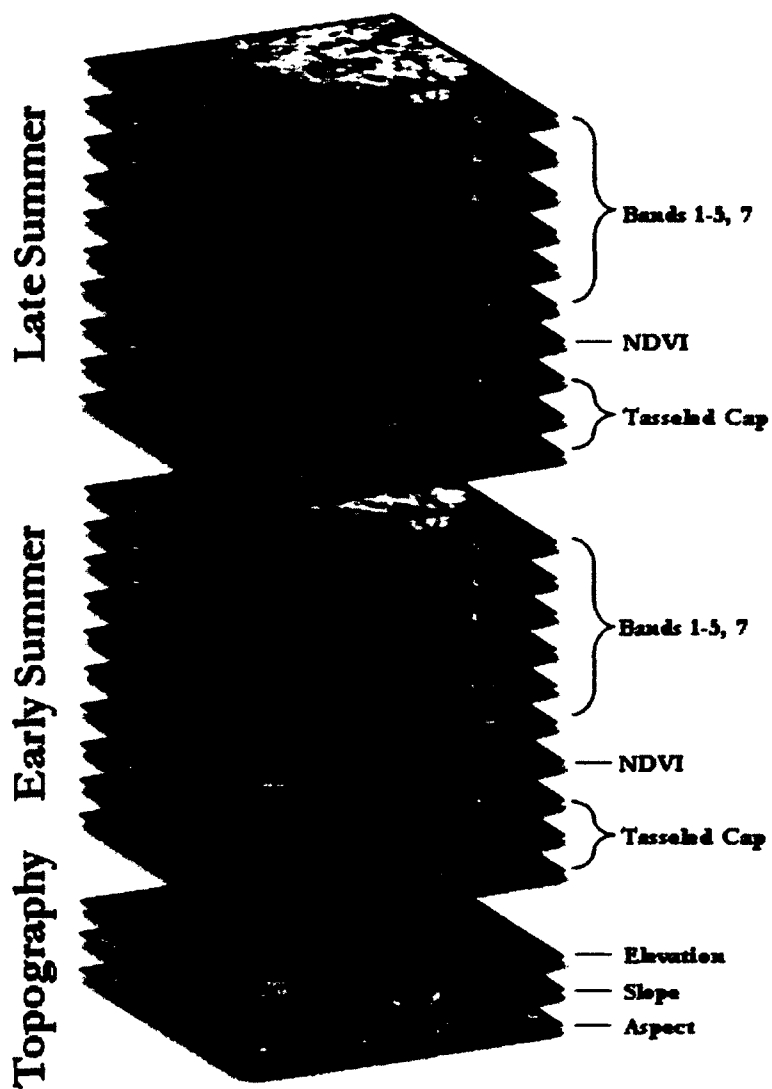


Figure 3. Contents of 23-band image

Segmentation Parameter Analysis and Land Cover Classification

All subsequent image processing and classification took place using Trimble eCognition Developer 8.7. An analysis was performed to determine the optimal segmentation parameters needed to attain the highest land cover classification accuracy. Of interest in the segmentation process were three parameters: (1) scale, (2) shape, and (3) color. The 23-band 2011 image was loaded into eCognition. Using the software's multiresolution segmentation algorithm, a series of image segmentations were performed. Assigning equal weights to all 23 spectral, derivative and topographic bands, the image was segmented at every combination of the following parameter settings:

- Scale 2-20, intervals of 2
- Shape 0.0-0.5, intervals of 0.1

(Note: given the tradeoff between shape and color parameters, a shape range of 0.0-0.5 is the same as a color range of 0.5-1.0)

There were a number of considerations that went into the determination of these test ranges. In terms of scale, a visual exploration of images segmented at a variety of scales facilitated the determination of 20 as a suitable high-end extreme. Beyond a scale of 20, the segments became exceedingly large and quickly began to lose their within-segment land cover homogeneity. In other words, at a scale of 30, for example, a single polygon could contain Forest, Shrub/Scrub *and* Grassland. In terms of shape/color, it was believed that spatial qualities of a segment (shape) should never have a stronger influence on determining the size and shape of the segments than the 23 "spectral" bands

(color). Accordingly, the high end of shape influence was determined to be 0.5 or 50% of the segmentation weight.

Each of the resulting segmentations was examined closely for the input parameters' effects on segment size, and other spatial and spectral characteristics. Of interest to this study was not only the general effect of scale parameter on segment size, but also the relative variation in segment size that resulted at each scale level. Accordingly, an analysis was performed to explore the relationship between segment size relative standard deviations (RSD) and the scale parameter. Because the segment sizes at large scale parameters will have significantly larger standard deviations, the normalized or relative standard deviation was deemed an appropriate representation of *within scale* segment size variation. RSD was calculated as such:

$$RSD = \frac{s_{ij}}{\mu_{ij}}$$

Where s_{ij} is the sample standard deviation of segment size (in pixels) at a given scale parameter i and shape parameter j , and μ_{ij} is the mean size at those same parameters. The mean RSDs by scale parameter were then calculated.

Each of the image segmentations then underwent a separate land cover classification. Land cover classifications were performed in both a pixel- and object-based environment, using a non-parametric classification algorithm (CART) and a parametric classification algorithm (Bayes). Taking into account all of the segmentation and classification permutations, 240 classifications of the 2011 imagery were performed (10 scale x 6 shape x 2 environments x 2 algorithms = 240 classifications in total). An

important distinction between what was being tested in the pixel- and object-based environments must be made here. For both pixel- and object-based classifications, image segments were intersected with training data sample unit centroids (as created through field reconnaissance and photo interpretation) to determine segment training units. In both cases, the classification algorithm was trained with the resultant image segment sample data. In the object-based environment, this trained model was then applied to the remaining, unclassified image segments. In the pixel-based environment, however, the trained model was then applied to the remaining, unclassified pixels on the image, effectively ignoring the boundaries of the remaining segments. So, in essence, the impact of the segment characteristics is twofold impact on the resultant classification accuracy (training samples *and* segment classification) in the object-based environment.

.In the pixel environment, however, the impact is singular, merely affecting the nature of the training data. Additionally, in the object-based environment, a host of segment features can be used to both train the model and classify the imagery, whereas pixels rely purely on the training data's per-band mean values and variances. The input features for object-based analysis were as follows:

- Mean layer value for each of the 23 bands by object
- Standard deviation
- Skewness
- Brightness
- Maximum pixel value
- Minimum pixel value
- Mean of object inner border

- Mean of object outer border
- Contrast to neighboring pixels
- Mean difference to neighboring objects
- Hue, saturation, intensity transformations (early & late)
- GLCM homogeneity
- Area
- Border length
- Compactness
- Roundness
- Rectangular fit
- Shape index

Accuracy Assessment

All of the resultant classifications underwent an accuracy assessment to determine which combination of segmentation parameters, analytical environment and classification algorithm attained the highest accuracies. Each of the 240 classifications was assessed using the traditional error matrix (Congalton *et al.*, 1983). Overall accuracies, class-specific user's and producer's accuracies, and Kappa were all calculated using these matrices (Congalton and Green, 2009). Additionally, an area-based error matrix (MacLean and Congalton, 2012) was used for the 120 object-based classifications. The resultant accuracies were compared to those computed using the traditional error matrix. For each combination of CART vs. Bayes and object vs. pixel, a mean overall accuracy was computed across each scale and shape parameter. The combined settings that

produced the highest average accuracy were then selected for use in all subsequent classifications. Upon completing the highest accuracy classification at each temporal interval, a simple thematic data post-processing took place whereby areas below the minimum map unit of 4,500 m² were removed and replaced with those surrounding land cover classes who shared the largest boundary with this area.

Land Cover Change

Change Detection

For a graphical depiction of the change detection process, see Figure 4 below.

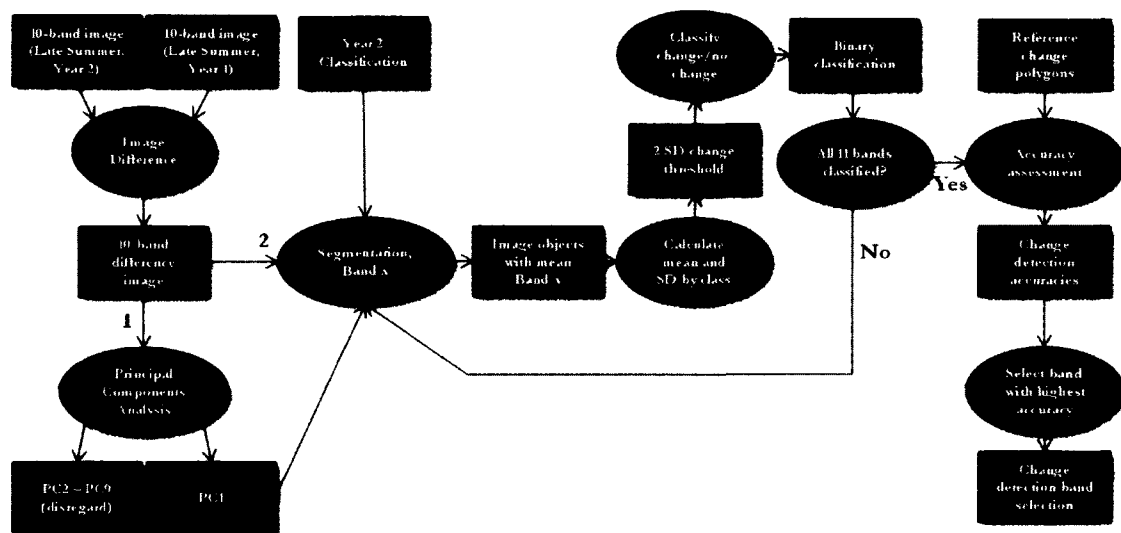


Figure 4. Change detection flowchart

In order to assess changes in the land cover, an image differencing was performed. For each 5-year interval of interest, the late summer, 10-band (6 raw spectral bands, 1 NDVI, TC1, TC2, TC3) image was used to create a 10-band difference image based on a simple pixel-by-pixel subtraction between one time period and the previous.

A principal components analysis (PCA) was performed on the 10-band difference image to reduce the change vectors to a single principal component (PC1) that would account for most of the variability found in all 10 bands. The resultant eigenvalues were used to compute the amount of change variation captured in PC1. Each of the 10 difference bands and PC1 were added into eCognition for further analysis. Using the highest accuracy 2011 classification as a thematic layer whose land cover polygons would form the boundaries for segmentation, a series of multiresolution segmentations took place. In each case, a single change layer was given the full segmentation weight. What resulted was 11 separate within-land cover class segmentations (6 spectral, 1 NDVI, 3 TC, 1 PC) with which band-specific change thresholds could be calculated. Using two standard deviations from the mean as a default threshold for delineating change areas, segments were classified in binary fashion into change and non-change areas based on their mean difference band values and land cover classification. The 11 different change area delineations were exported as a polygon shapefile to be assessed for change detection accuracy in ArcGIS 10.

Change reference polygons were manually digitized in ArcMap 10 in the following manner. The 10-band 2011 late summer image and that from 2006 were loaded into ArcMap. These images were then visually analyzed to determine an area appropriate for change detection accuracy assessment, again, focusing on land cover changes primarily related to forest harvesting. A roughly 15,000 ha area in northern Union County where significant logging activity had taken place during this interval was selected for further analysis. Through the use of a variety RGB band composites including visible (3, 2, 1), false-color near-infrared (4, 3, 2), and a variety of other

combinations that appeared well suited to detect forest cover change, areas of significant change were digitized on screen at a scale of 1:15,000. Each of the automated change area delineations was then clipped to the same rectangular extent of the reference area. Each was subsequently unioned with the reference change-no change classification and areas of commonality and difference were calculated in hectares to determine the degree of thematic spatial agreement between reference data and map data. Each dataset was then analyzed using a 2 x 2 change-no change error matrix (Congalton and Green, 2009) to calculate overall accuracies, user's accuracies (errors of omission) and producer's accuracies (errors of commission) for change areas. Of interest to this study were change detection algorithms with high overall accuracies, and similar user's and producer's accuracies (in the interest of avoiding vast over- or under-estimation of change). If unequal, then a greater weight was given to higher producer's accuracies (commission errors, for the purposes of this project, are preferable to omission errors, if only slightly so). The highest accuracy change detection band was then selected for further analysis.

Given the relatively high overall omission errors using the two-standard deviation threshold across all bands, an analysis of optimal threshold selection was performed using the most accurate single-band change detection method. Assuming that higher thresholds would only result in greater omission errors, four smaller standard deviation-based thresholds were tested for change detection accuracy: 1 SD, 1.25 SD, 1.5 SD and 1.75 SD. Using the same change detection accuracy methods described above, the highest accuracy threshold was chosen for use in the change detection and subsequent classification process.

Change Classification

For a graphical depiction of the change detection process (as described by the C-CAP change classification protocol, Dobson *et al.*, 1995), see Figure 5 below.

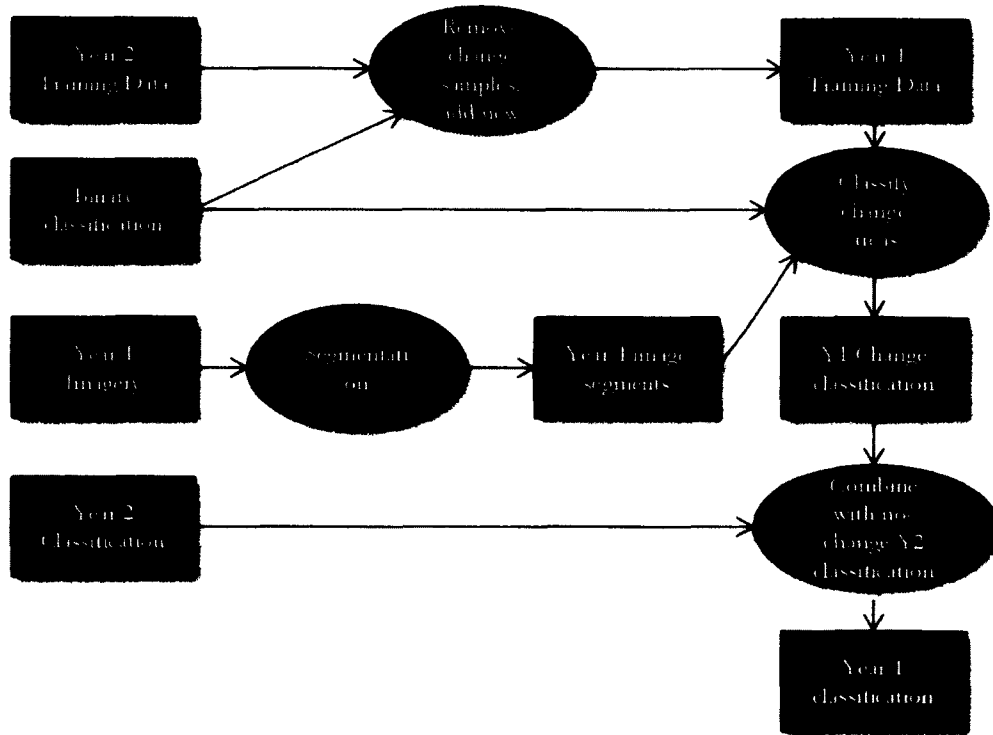


Figure 5. C-CAP change classification flowchart

With the optimal change detection methodology in place, a full change classification was able to be performed. The first step in the classification process entailed manipulation of the training data. It can be assumed, for example, that the training data for 2011's classification is still valid in those areas that were classified as non-change. However, those training samples that fell within change areas must be adjusted accordingly. In order to maintain the same total and class-specific numbers of

training samples, the invalid training samples were removed and subsequently replaced through a visual interpretation of the 2006 imagery.

For the 2011-2006 change classification, the 23-band 2006 image was added to eCognition. The image was segmented, again, with equal weight given to all 23 bands using the pre-determined optimal single-time segmentation parameters and the multiresolution segmentation algorithm. Importantly, however, the image was only segmented *outside of* the change areas. In other words, only those areas that were classified as non-change were segmented. The polygons that represented change remained intact. Following the same protocol as the 2011 classification, the resultant segments were classified using the training sample centroids. These sample segments were then used to train the classification model. Instead of classifying the entire image wall-to-wall, however, only those areas that were previously established as change areas were classified. The resulting change area classification was then merged with the 2011 classification to form a wall-to-wall classification for 2006. The same process, from change detection to training data manipulation, classification and merging took place for every interval of interest. Additionally, the same change detection accuracy assessments were performed on each interval, comparing the automatically-detected change areas to manually digitized areas of similarly high logging activity.

Lastly, all of the land cover classifications were compared by 5-year interval to determine the changes that have occurred in the landscape. Change matrices were created by performing a simple spatial intersection between land cover classifications and subsequent area calculations. Additionally, these changes were intersected with polygons representing broad land ownership classes, including public lands, private industrial lands

and private non-industrial lands. As the changes in the forested environment are of key importance to this study, the 6 x 6 land cover change matrices were reduced to simple 2 x 2 forest-non forest matrices to assess forest harvesting and regeneration trends, both across the entire landscape and across different ownership classes.

CHAPTER III

RESULTS

Segmentation Parameter Analysis and Land Cover Classification

The scale segmentation parameter has a significant and direct effect on resultant image segment size. For a qualitative, visual account of the stark contrast between image segmentations performed at the extreme ends of this study's test range (2 and 20), see Figure 6. As can clearly be seen in these images, the implications of using different segment sizes for training data (in both the pixel- and object-based analysis) and for subsequent land cover classification (in the case of object-based analysis) should not be ignored. In areas of high spectral variation, such as the urban area in the southeastern portion of the image, the scale=2 segmentation produced segments in some cases as small as a single pixel. As such, an object-based classification with these small segments is in many ways comparable to a pixel-based classification. Conversely, in the scale=20 segmentation, the massive resultant segments are perhaps too spectrally inclusive, where multiple land cover types could potentially fall in a single segment.

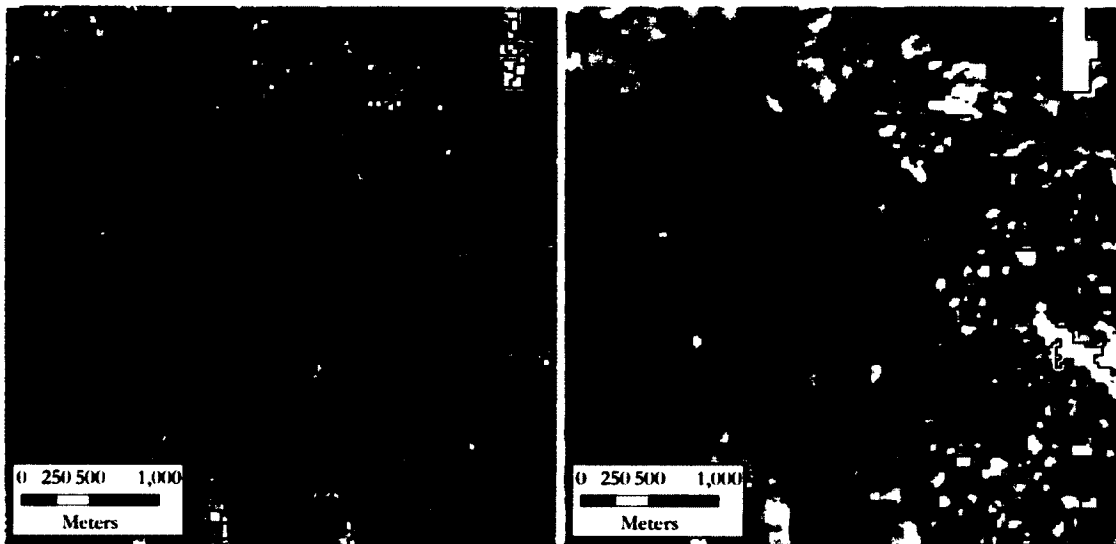


Figure 6. A subset scene of northwestern La Grande, Union County, OR segmented at scale parameters of 2 (left) and 20 (right)

In order to obtain a quantitative estimate of the impact of the scale segmentation parameter on resultant segment size, an analysis was performed using the accuracy assessment sample data. For each segmentation performed at incremental levels of the scale parameter, the accuracy assessment sample data were used to obtain a mean value of segment size (in pixels). Given the fact that accuracy assessment data are deemed to be a statistically robust thematic and spatial representation of the entire dataset, it was assumed that the segment sizes of the accuracy data were similarly representative. Figure 7 contains 60 data points of segment size displayed by scale parameter, each point representing a different shape parameter input. A power function trendline was fitted to the model and a R^2 value was computed. As can be seen, there is a fairly directly positive relationship between scale parameter and segment size. This is to be expected. Interestingly, this relationship is not linear, but exponential. It should be noted, however, that this study concluded its high end segment size analysis at a scale parameter of 20. In

reality, segmentations can be performed at much higher scale levels than 20. Beyond a certain value, it is believed that the distribution of resultant segment sizes would reach an asymptote. Where that leveling off occurs, however, will vary dependent upon the spatial extent and spatial resolution of the imagery.

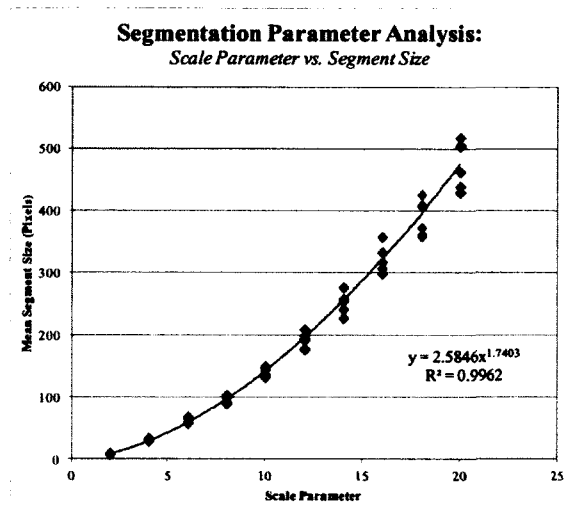


Figure 7. The effect of scale parameters on resultant segment size

A test was performed to explore the relationship between the scale parameter and segment size variability, as measured by the segment size RSD. The results of this test can be seen in Figure 8, where two notable trends emerge. The first is a peak RSD at the lowest scale parameter of 2 (RSD = 1.03). This suggests that at a scale of 2, fairly high variability in segment size can be expected. This trend declines to a trough at scale of 8, where segment size was the most consistent. Following this low RSD, a slow steady rise in variability emerges as the segment size increases. Again, it is worth noting that the behavior of this trend *beyond* a scale of 20 is unpredictable based on these results.

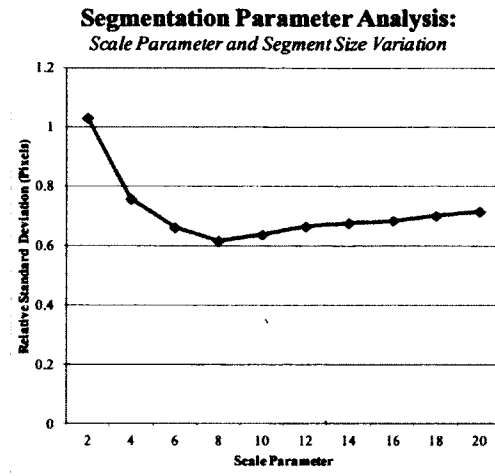


Figure 8. The effect of scale parameters on variation in resultant segment size

The manipulation of the shape parameter did not result in a predictable distribution of segment sizes. Instead, the tradeoff between shape and color parameters primarily affected the segments' spatial and spectral characteristics, as is their nature. Again, the results are fairly predictable. Figure 9 represents the same subset scene from Figure 5 segmented at a consistent scale of 10 but with a varying shape parameter. As can clearly be seen, the segments that result are significantly visually distinct from one another. The shape 0.0 (color 1.0) segmentation has clearly grouped together pixels of similar spectral quality and largely ignored the compactness and smoothness of the resultant segments. Conversely, the shape 0.5 (color 0.5) segmentation has produced much more compact, smoother segments by grouping together areas covering a larger distribution of spectral qualities.

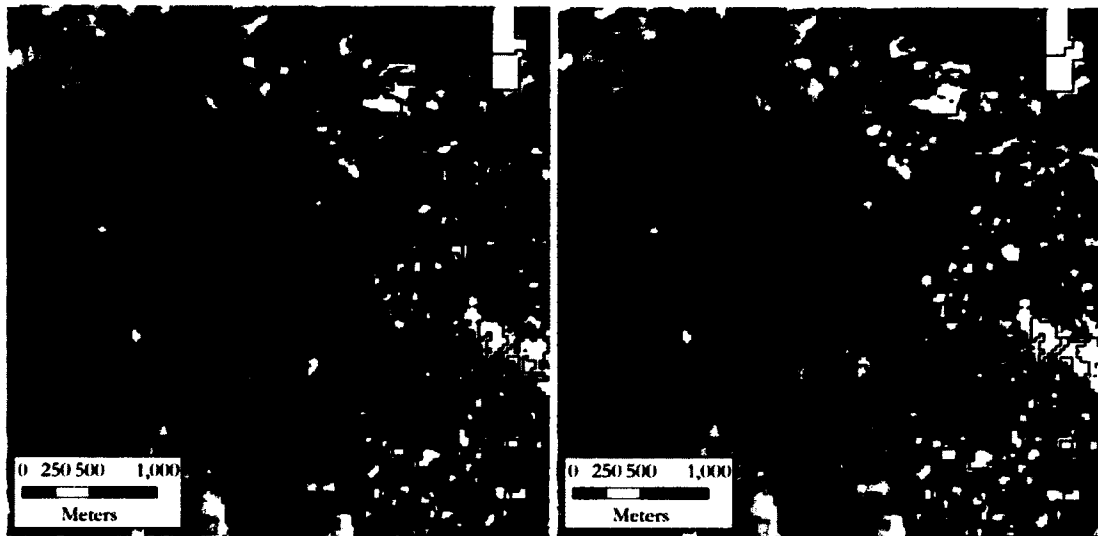


Figure 9. A subset scene of northwestern La Grande, Union County, OR segmented at shape parameters of 0.0 (left) and 0.5 (right)

For every combination of scale and shape parameter segmentations, a classification was performed using all four combinations of CART vs. Bayes and pixel-based vs. object-based classification. Henceforth, CART object-based = CO, CART pixel-based = CP, Bayes object-based = BO, and Bayes pixel-based = BP. As a result, 240 classifications in all were performed and their thematic accuracies were assessed using the traditional error matrix (Congalton *et al.*, 1983). The overall accuracies for CO, CP, BO and BP were averaged for each different scale parameter segmentation. The resultant mean accuracies can be seen in Figure 10. A few clear trends emerge. First of all, in all cases BP produced the highest classification accuracies, with a peak at a scale parameter of 8, where the mean overall accuracy was 90.68%. Although not very strong, the relationship between scale and BP accuracy certainly does take on a fairly consistent trend. With an additional increasing trend seen towards the high-end scale parameter of 20, perhaps higher classification accuracies than those produced at a scale of 8 could

have been attained. Interestingly, CP, also pixel-based, although consistently less accurate than BP, shares a similar trend, albeit less smooth, with a peak occurring at or around a scale of 8 and a trough at 18. The two object-based classifications, CO and BO similarly share a generalized trend in accuracy across the range of scale parameters. In both cases, there appears to be a fairly distinct positive relationship between scale and overall classification accuracy. The relationship is certainly stronger in BO than in CO, but in BO there is a sharp decrease in accuracy at the very last scale parameter tested, 20. While BP greatly outperformed CP, CO almost exclusively outperformed BO, if only slightly.

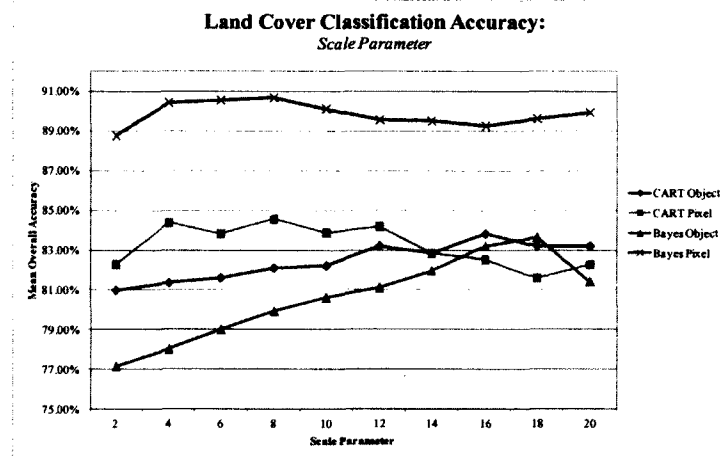


Figure 10. Average overall accuracies of CO, CP, BO and BP across the range of scale parameters

Similarly, the overall accuracies for CO, CP, BO and BP were averaged for each different shape parameter segmentation. The resultant mean accuracies can be seen in Figure 11. It is important to note that Figures 10 and 11 should be considered together, rather than in isolation of one another, particularly when comparing *between*

classification method accuracies, because these results tend to be similar across the entire ranges of scale and shape parameters, with the order of descending accuracy being roughly equivalent to BP (best), CP, CO, and BO (worst). That being said, these graphs do function as good indicators of *within classification method* accuracies. The trend lines of scale vs. accuracy themselves are believed to be the most revealing. Accordingly, some important trends emerge in Figure 11 as well. The most accurate method, BP, appears to function almost entirely independent of shape, with functionally equal accuracies across the board. That being said, the marginally highest mean accuracy was produced at a shape parameter of 0.3 (89.96%). Conversely, CP, CO, and BO all appear to have an accuracy peak in the 0.1-0.3 ranges and a trough in the 0.4-0.5 range, with a slight uptick in accuracy at shape 0.5.

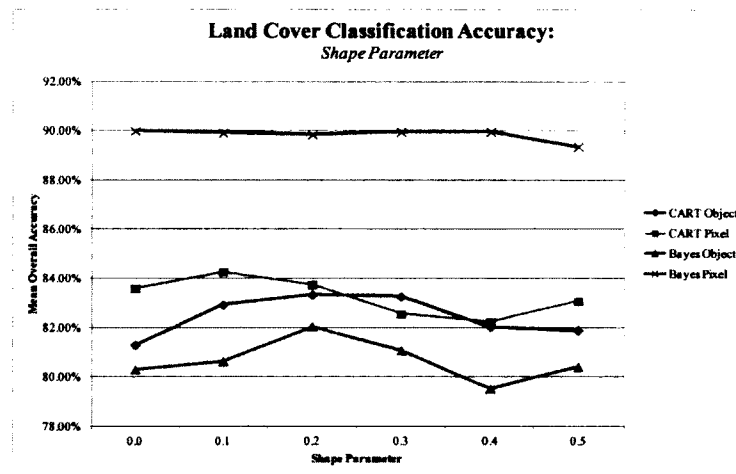


Figure 11. Average overall accuracies of CO, CP, BO and BP across the range of shape parameters

Taking all of these accuracies into consideration, a selection of segmentation parameters (scale and shape), image analysis environment (pixel vs. object) and

classification algorithm (CART vs. Bayes) was made. The optimal combination was found to be Bayes pixel-based classification with training samples segmented at a scale of 8 and a shape of 0.3. In addition to the highest *mean* overall accuracy distributed across an array of shape parameter inputs, this combination of settings actually produced the highest single-time accuracy as well, with an overall accuracy of 91.48% (Kappa = 0.897). The error matrix with class-specific user's and producer's accuracies can be seen in Table 4. In addition to performing well overall, none of the classes had user's or producer's accuracies of lower than 80%. Water and forest classification performed particularly well with equal user's and producer's accuracies of 100% and 98%, respectively. These estimates reflect the accuracies of the raw classified data. After performing majority filter to eliminate noise, the accuracies were increased. These values can be seen in Table 5. The final 2011 land cover classification can be seen in Figure 12.

		Reference Data						Sum Units	User Accuracy
		1	0	1	0	0			
Map Data	1	4	0	2	0	0	45	95.56%	
	0	0	0	0	1	0	43	86.05%	
	2	1	1	0	1	0	50	98.00%	
	1	1	0	7	0	0	45	88.89%	
	0	0	0	0	0	0	57	84.21%	
	0	0	0	0	0	3	30	100.00%	
Sum Units		50	40	50	50	50	30	270	
Producer Accuracy		86.00%	92.50%	98.00%	80.00%	96.00%	100.00%		91.48%

Table 4. Error matrix of highest accuracy land cover classification *before* post-processing

		Reference Data						Sum Units	User Accuracy
Map Data		0	0	1	0	0	44	97.73%	
	4	0	0	1	0	0	42	88.10%	
	0	0	0	0	1	0	50	98.00%	
	2	1	1	0	1	0	47	89.36%	
	1	2	0	6	0	0	57	84.21%	
	0	0	0	0	0	30	30	100.00%	
Sum Units	50	40	50	50	50	30	270		
Producer Accuracy	86.00%	92.50%	98.00%	84.00%	96.00%	100.00%		92.22%	

Table 5. Error matrix of highest accuracy land cover classification *after* post-processing

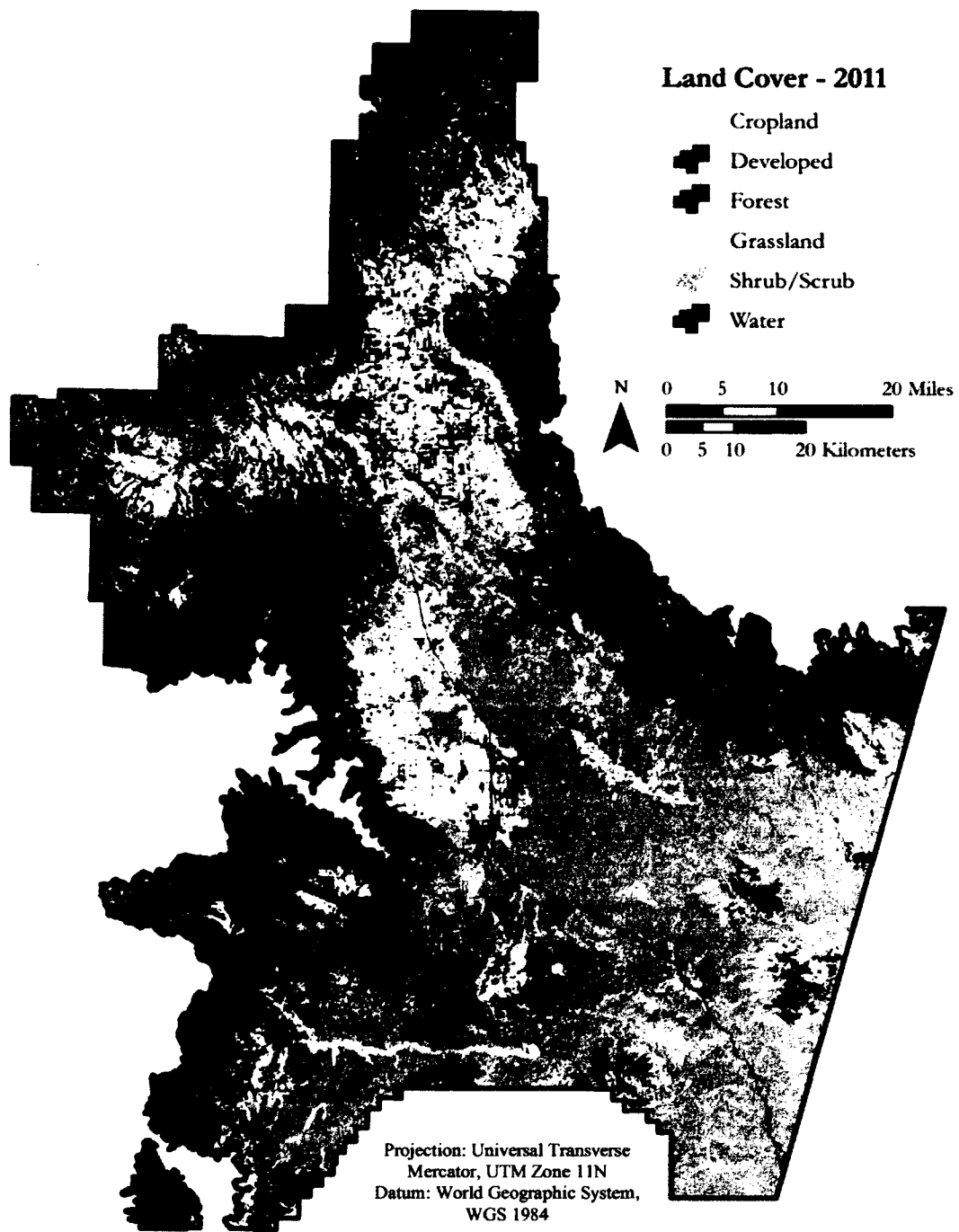


Figure 12. 2011 land cover classification

Accuracy Assessment

For each of the 120 object-based land cover classifications, two measures of accuracy were computed. The first, which were reported earlier, were accuracies as estimated by the traditional sample unit-based error matrix. The second series of accuracy assessments was performed using an area-based error matrix. Instead of accuracies based on sample unit totals, this matrix uses sample unit segment size as an estimator of accuracies. Of particular interest were the differences between traditional and area-based accuracies and error estimations. Figures 13 and 14 highlight these differences. In Figure 13, the two overall accuracy estimation techniques and results are displayed by scale parameter for the CART classifier (A) as well as the Bayes classifier (B). In both cases, the area-based error matrices consistently report higher accuracies than the traditional matrices. In 13A, the differences are perhaps not as stark as in 13B, but interesting results emerge nonetheless. In particular, between the scale range of 2-8, area-based accuracies decline with increasing segment size, whereas unit-based accuracies increase. In 13B, the differences between methods are highest in the scale range of 4-10, where significantly higher area-based accuracies emerge. As scales increase beyond this range, however, the differences decrease until a scale of 20 where the differences are null.

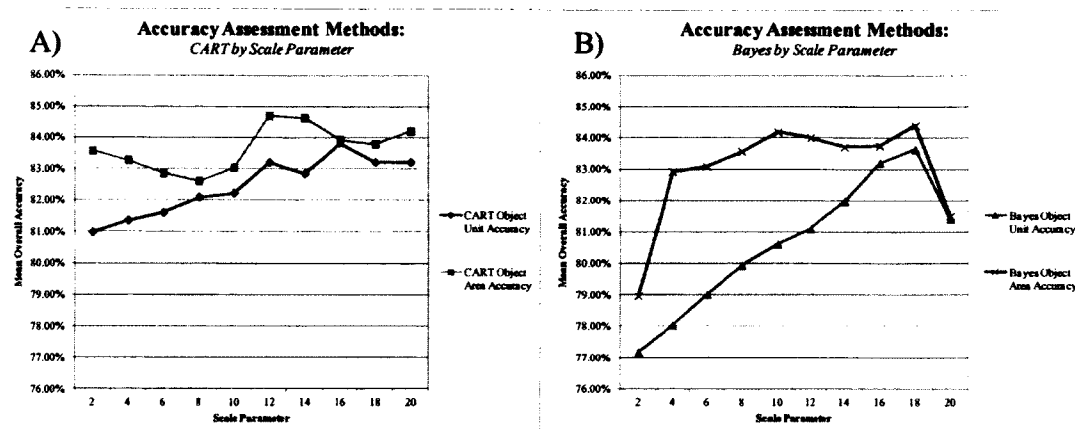


Figure 13. Overall accuracies estimated using unit-based and area-based error matrices by scale parameter for CART (A) and Bayes (B)

In Figure 14, the two overall accuracy estimation techniques and results are displayed by shape parameter for the CART classifier (A) and the Bayes classifier (B). With one minor exception, again in both cases, the area-based error matrices consistently report higher accuracies than the traditional matrices. The one exception that occurs can be seen in Figure 14A, where with a shape parameter of 0.5, the traditional unit-based error matrix reported a slightly higher overall accuracy. On the other end of the spectrum, the area-based accuracy appears to diverge from the unit-based accuracy, with a reported ~3% difference in mean overall accuracy. According to the Bayes accuracies in Figure 14B, the area-based accuracies are consistently significantly higher than the unit-based accuracies with few notable shape-based trends in difference.

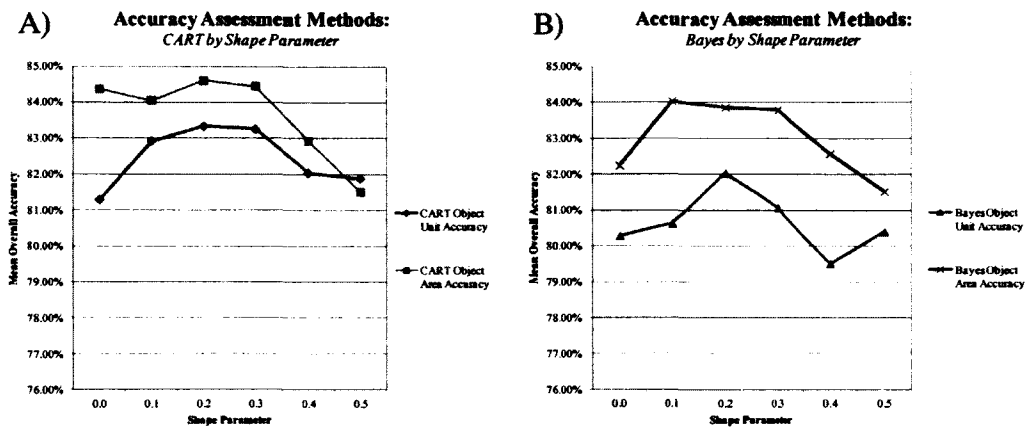


Figure 14. Overall accuracies estimated using unit-based and area-based error matrices by shape parameter for CART (A) and Bayes (B)

In order to quantify the differences in unit- and area-based error matrix accuracies, the absolute values of the differences between the two were averaged by scale parameter. This information was then combined with the segment size variation information from Figure 8 to highlight any potential connections between the variability in segment size and the differences in accuracies that may result. This combined information can be seen in Figure 15. Looking first at the absolute differences in CART accuracies, it appears that the relationship between accuracy difference and scale parameter are not very strong. That being said, there does appear to be a similar pattern to the segment size variation and the differences in CART accuracies. Both have a peak at a scale 2 and slope downward to a trough at scale 8. The trends between scale 8 and scale 20 appear less precisely related, yet still share similar steady increases. Conversely, the differences in Bayes accuracies seem to act entirely independent of segment size variation, and instead appear to have a strong negative correlation with scale parameter. That is, as the scale parameter (segment size) increases, the differences in reported overall accuracies between the unit- and area-based error matrices decrease.

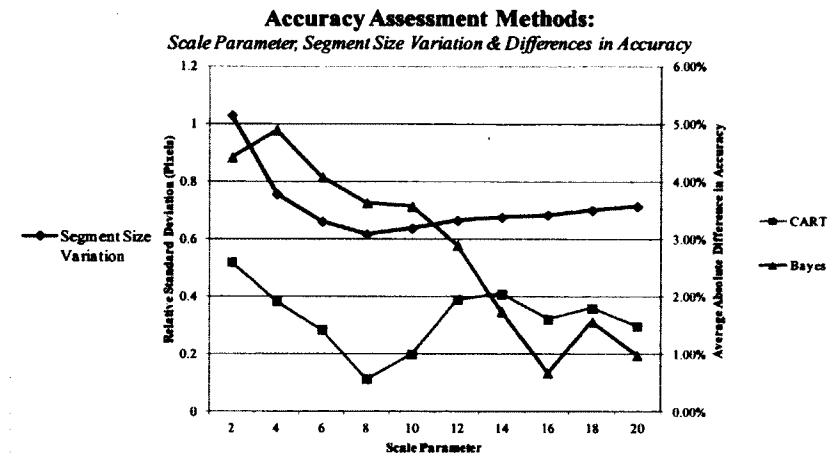


Figure 15. The effect of segment size variation on differences in unit- and area-based error matrix accuracies

Land Cover Change

To determine the optimal change detection technique, the first change interval of interest, 2006-2011 was used as a basis of operation. Ten different difference images and one principal components image were tested for their resultant change detection accuracy. The PCA was performed on the 10-band difference image to capture as much change across all of the input bands as possible into a single band. The 10 eigenvalues and computed change variance percentage captured can be seen in Table 6. As can be seen, almost 70% of the change variance is captured in PC1.

1	1036.87	69.87%
2	253.17	17.06%
3	130.11	8.77%
4	42.78	2.88%
5	6.38	0.43%
6	5.49	0.37%
7	4.10	0.28%
8	2.39	0.16%
9	1.58	0.11%
10	1.07	0.07%

Table 6. Principal components analysis of 10-band difference image with accordant eigenvalues and variance computations

Using the highest accuracy, post-processed 2011 land cover classification, a within-class segmentation was performed for each of the 11 change bands of interest (10 difference bands and PC1). From the resultant segments, a distribution of class-specific change values emerged, similar to those seen in Figure 16. For each band and class, the change distributions resembled a normal distribution. Importantly, however, the class-specific differences can be seen in the spread of change magnitudes. For instance, in Figure 16, the change distribution is much wider for Cropland than it is for Forest, which makes sense given that an undisturbed forest sees little spectral change from one year to the next, while the very definition of cropland implies its constantly modified vegetative cover. In order to determine change thresholds, the class-specific change means and standard deviations were calculated for each band. These values can be seen in Table 7. It should be noted that these mean values represent a digital layer rescaled from float single format to unsigned 8-bit. As a result, instead of a mean at or near 0 (no change), the values vary somewhere in the mid-100s.

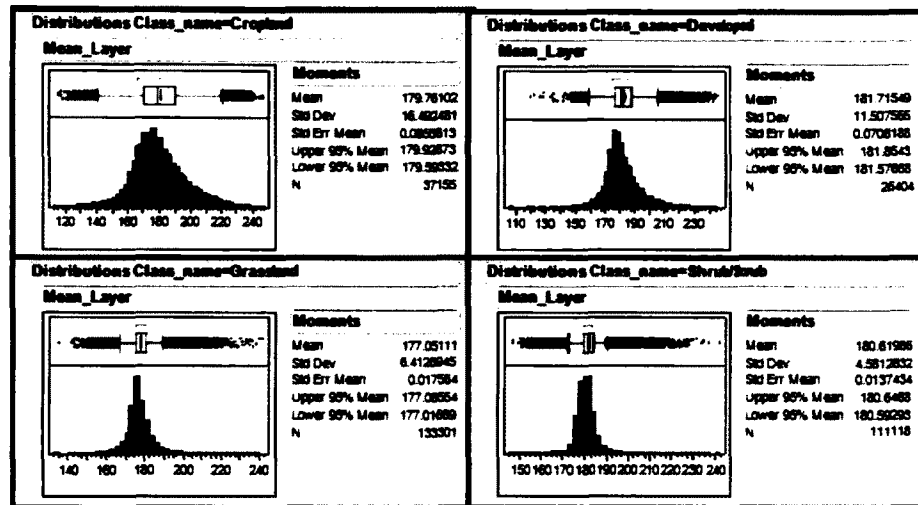


Figure 16. Example class-specific difference image value distributions

	Mean	SD																				
Cropland	174.93	10.25	171.29	11.89	171.95	19.49	139.36	23.36	167.79	19.65	157.31	14.30	132.75	16.08	177.18	16.05	111.67	39.60	137.21	25.84	180.26	16.49
Developed	174.81	8.73	171.50	8.83	172.96	12.84	139.93	14.56	165.16	13.91	154.48	10.40	131.36	10.39	175.34	12.72	97.23	25.79	142.26	16.95	181.86	11.75
Forest	170.09	2.05	164.16	2.09	163.69	3.05	133.49	3.67	158.06	5.82	152.53	3.35	133.69	4.90	161.77	4.15	96.48	7.49	144.54	6.71	172.54	2.73
Grassland	172.30	3.83	167.23	4.39	167.68	6.76	134.67	7.95	162.03	10.51	154.16	6.68	131.75	6.85	168.66	7.80	94.33	16.87	140.86	11.64	177.03	6.40
Shrub/Scrub	173.28	3.06	168.93	3.73	169.47	5.14	133.73	5.61	162.57	6.15	154.32	4.50	130.48	4.49	170.21	5.94	80.30	8.34	139.85	7.27	180.57	4.93
Water	173.90	7.07	168.79	7.23	169.74	10.01	140.32	15.42	169.07	19.73	159.90	13.08	126.14	31.09	169.68	15.93	93.05	20.05	139.62	17.80	178.15	16.07

Table 7. Mean and standard deviation of difference image values by land cover class

Using two standard deviations from the mean as a base threshold for change, each band was tested for its ability to accurately detect change. These class-specific band threshold values were applied to the binary classification of change versus non-change for the 2006-2011 interval. As a result, 11 different classifications were performed. Each classification underwent an accuracy assessment. Following a spatial intersection between the map data and the reference data, areas of commonality and disparity were computed in hectares. These were then compiled and analyzed in error matrices to determine change area commission and omission, overall accuracy and Kappa (See Appendix B for band error matrices). The user's and producer's accuracies are proxies for

commission and omission errors, respectively. The results of change detection commission and omission can be seen in Figure 17. Among all of the bands tested, the PCA band detected the greatest amount of change within the area of interest (1,722 ha). While the total reference change area was equal to 1,945 ha, 413 ha of the PCA-detected change was classified in error. As a result, the PCA had a user's accuracy of 76.01%. The highest user's accuracy was achieved using the NDVI difference image (83.74%). Accordingly, the NDVI had the lowest commission error. In terms of omission error, band 7 was found to have the highest producer's accuracy (73.22%). Out of the 11 bands tested, the PCA performed 3rd best, with a producer's accuracy of 67.33%, following band 5 with a producer's accuracy of 72.62%. Notably, in terms of omission error, the PCA outperformed all other derivative bands tested (NDVI and 3 TC features).

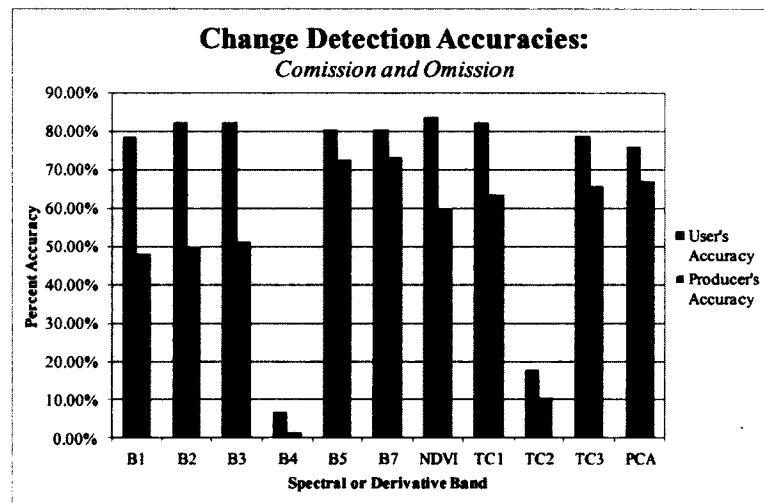


Figure 17. User's and producer's accuracies of change areas detected using different spectral and derivative bands

In addition to user's and producer's accuracies for change detection, Kappa was calculated in order to assess overall model performance. Given the fact that the sheer

magnitude of the non-change areas in the reference data greatly outweighed the change areas, Kappa was deemed to be a more robust estimator of overall performance than the inflated overall accuracy calculation. The resultant Kappa values can be seen in Figure 18. Both band 5 and 7 clearly outperformed any others. Band 7 edged out band 5, however, with Kappa values of 0.737 and 0.735, respectively. Band 4 performed exceedingly poorly, with a Kappa of -0.019, suggesting an agreement occurring less than predicted by chance alone. TC2 (greenness) likewise performed poorly, which makes sense given band 4's strong influence on this portion of the Tasseled Cap transformation. PCA (Kappa 0.679) outperformed NDVI, but fell short of TC1 (Kappa 0.688) and TC3 (Kappa 0.685), if only by a small margin.

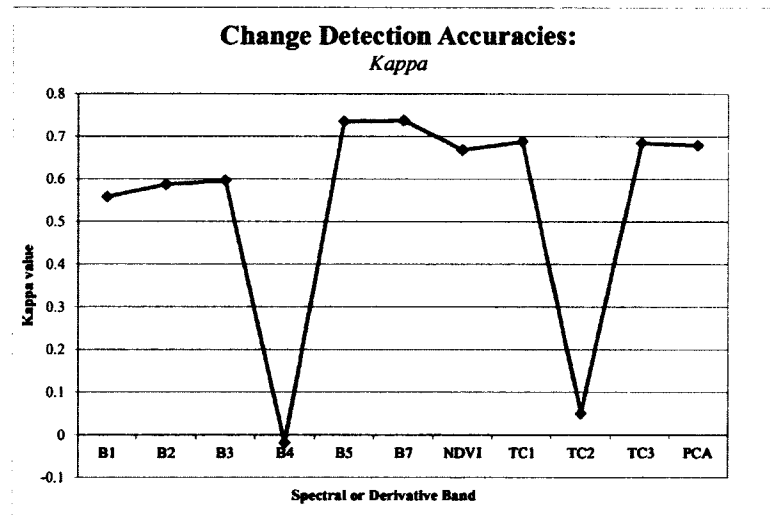


Figure 18. Kappa accuracy of change areas detected using different spectral and derivative bands

Given the preferential emphasis placed on minimizing omission errors (as opposed to minimizing commission), and the highest overall performance in terms of

Kappa, band 7 was deemed the optimal band selection for change detection. The change matrix for band 7 can be seen in Table 8.

		Reference		Sum Area	User
		1	2		
Map	1	348.30	15,116.67	1,772.07	80.34%
	2	520.86	14,944.12	15,116.67	96.55%
Sum Area		1,944.63	14,944.12	16,888.74	
Producer		73.22%	97.67%		94.85%

Table 8. Change detection error matrix for band 7, threshold 2 SD

Change omission and commission errors can be seen as a direct product of the change threshold used. In other words, a higher standard deviation-based change threshold will likely produce greater omission error and a lower threshold will produce increased errors of commission. Accordingly, band 7 was tested at a range of standard deviation change thresholds (1SD - 2SD, intervals of 0.25SD) (See Appendix C for threshold error matrices). The results of this test can be seen in Figure 19. As expected, user's accuracies decrease and producer's accuracies increase as the threshold level decreases.

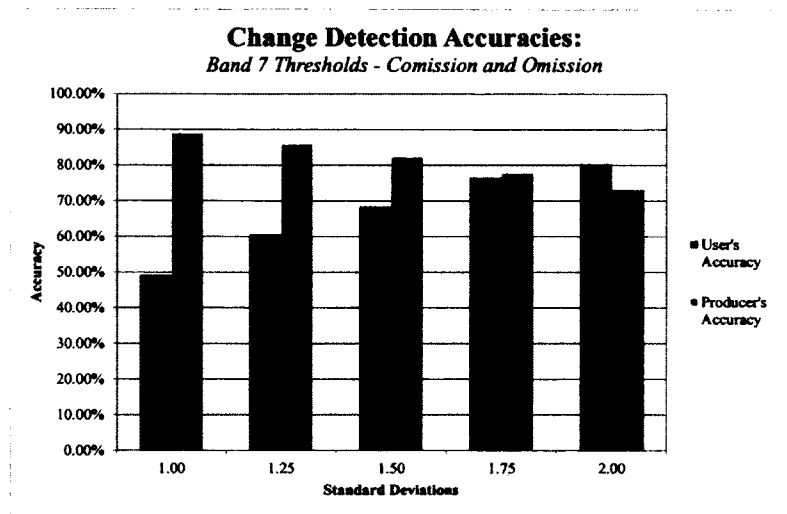


Figure 19. User's and producer's accuracies of change areas detected using band 7 at different standard deviation thresholds

Kappa was also calculated at each band 7 threshold level. These results can be seen in Figure 20. According to Kappa, a threshold of 1.75SD was found to be the best predictor of change (Kappa 0.7444).

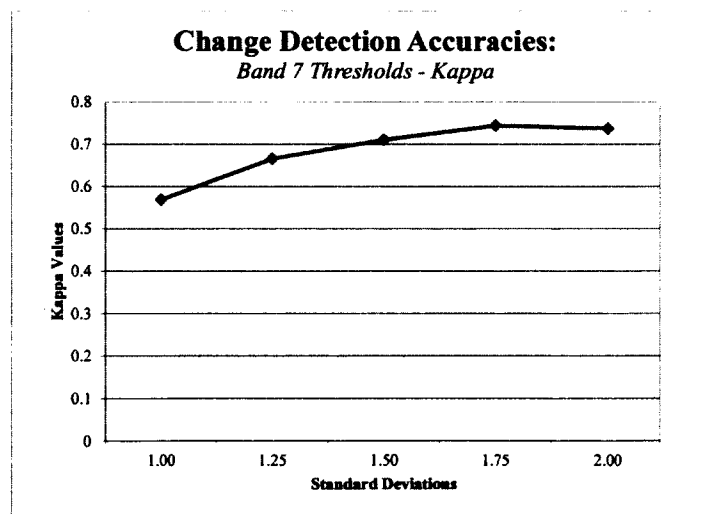


Figure 20. Kappa accuracy of change areas detected using band 7 at different standard deviation thresholds

Given band 7's superior performance at 1.75SD in terms of both Kappa and the tradeoff between user's and producer's accuracies (higher producer's than producer's accuracy without excessive overestimation of change), it was selected as the change threshold of choice for further use. Its change detection error matrix can be seen in Table 9.

		Reference		Sum Area	User
		Change	No Change		
Map	Change	415.69	1,772.07	76.54%	
	No Change	389.74	15,116.67	97.42%	
Sum Area		1,746.13	15,142.62	16,888.74	
Producer		77.68%	97.25%		95.23%

Table 9. Change detection error matrix for band 7, threshold 1.75 SD

Band 7 was used to classify change and non-change areas for each 5-year interval of interest iteratively backwards in time starting with 2006-2011 (results described above) and ending with 1986-1991. Using reference data hand-digitized in interval-specific areas of high logging activity, accuracy assessments were performed for each change detection analysis. The resulting change user's and producer's accuracies for each of these intervals can be seen in Figure 21. Notably, the producer's accuracies decline backwards in time from the 2006-2011 interval to the 1996-2001 classification. Although these accuracies begin to climb for the last two intervals, they never reach the level of the initial 2006-2011 change detection. Conversely, the highest user's accuracy is found in the 1991-1996 interval (86.39%). This value suggests very low commission errors at that interval.

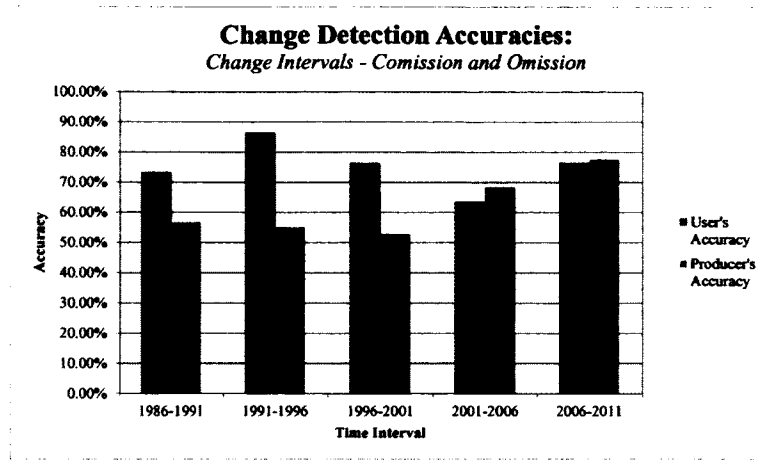


Figure 21. User's and producer's accuracies of change areas detected using band 7 at different time intervals

In addition to user's and producer's accuracies, Kappa was calculated at each temporal interval. The results of these assessments can be seen in Figure 22. Following a similar pattern to the change user's accuracy, the highest Kappa value was found for the most recent change detection (2006-2011, Kappa 0.7444) and the lowest for the interval of 1996-2001 (Kappa 0.589).

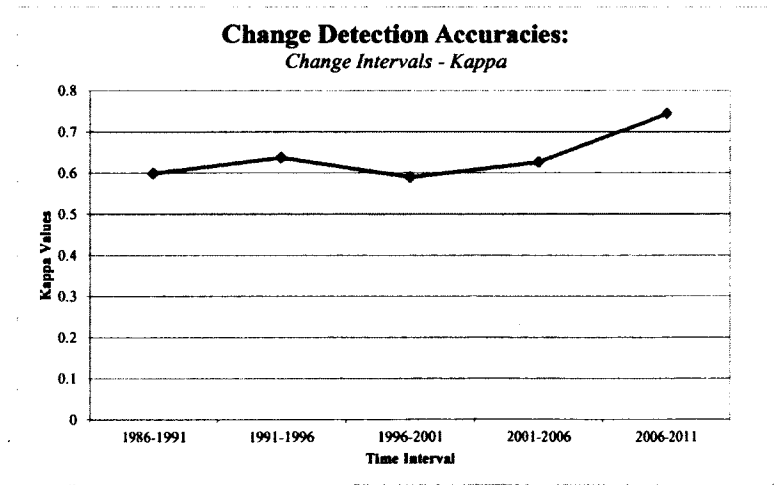


Figure 22. Kappa accuracy of change areas detected using band 7 at different time intervals

For each temporal interval of interest, land cover classifications were performed on the detected change areas. These change area classifications were then merged with the latter year's classification to attain wall-to-wall classification (See Appendix D for land cover totals). The resultant classifications were intersected to assess class-specific land cover classification changes. Areas were calculated in hectares to determine change magnitude. These 6 x 6 change classifications were simplified to forest and non-forest changes. Four combinations resulted: forest to forest (non-change), forest to non-forest (change), non-forest to non-forest (non-change), and non-forest to forest (change). After adjusting for natural disturbance events, forest to non-forest changes were assumed to be the result of harvesting and non-forest to forest changes were assumed to represent forest regeneration. These totals were then intersected with land ownership data to determine owner-specific changes. The forest to non-forest totals and ownership breakdown can be seen in Table 10 and Figure 23. A few definitive trends emerge. In terms of overall forest harvesting, the first two time intervals (1986-1991 and 1991-1996) saw very similar total hectares removed at slightly below 8,500 ha each. Following these early highs, a precipitous drop occurred in the 1996-2001 interval, where only 2,126 ha were removed in total. The final two intervals saw consistently increasing totals with 5,477 ha removed between 2001 and 2006 and 9,227 ha removed in the most recent interval, reaching the highest total of any interval tested. In terms of ownership-specific patterns, some clear trends can be seen as well. A notable decrease in harvesting on public land occurred between 1986 and 2001 (1986-1991: 6,242 ha; 1991-1996: 3,434 ha; 1996-2001: 749 ha), followed by a less aggressive, steady increase between 2001 and 2011.

Harvesting on private industrial land saw significant increases between the 1986-1991 interval (402 ha removed) and the 2006-2011 interval (3,975 ha removed). Private non-industrial land typically saw relatively low harvesting totals, with the one exception being between 1991 and 1996 where 3,603 ha were removed.

	<i>Private Industrial</i>	<i>Private Non-Industrial</i>	<i>Public</i>	<i>Total</i>
1986-1991	401.88	1,666.66	6,242.37	8,310.91
1991-1996	1,346.69	3,602.59	3,433.96	8,394.39
1996-2001	342.42	1,032.44	749.47	2,126.79
2001-2006	2,272.57	954.84	2,243.12	5,477.49
2006-2011	3,974.84	1,805.27	3,439.24	9,226.89

Table 10. Total harvesting by 5-year interval broken down by land ownership class

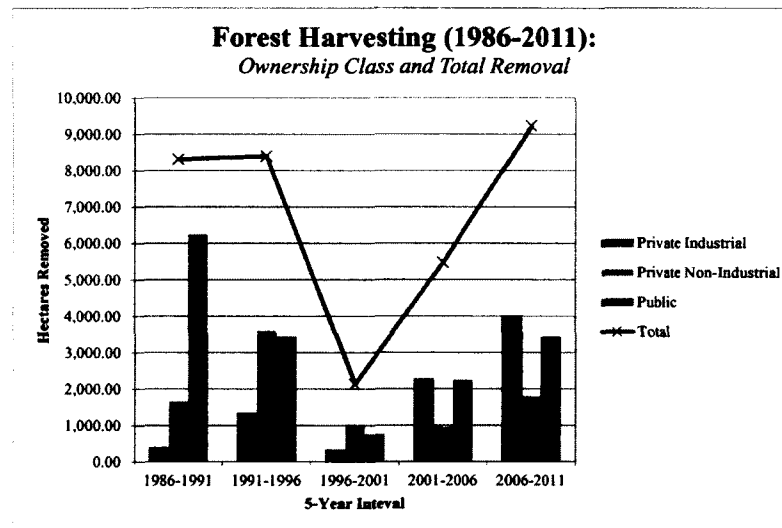


Figure 23. Total harvesting by 5-year interval broken down by land ownership class

These results however, should be viewed with the understanding of differential total forest land ownership. As can be seen in Table 11, for example, in 2011, there were 418,144 ha of forested land throughout the entire study area, 312,284 ha (74.68%) is

owned by public entities (most of which is USFS), followed by private non-industrial land owners (77,732 ha, 18.59%), and lastly, private industrial (28,127 ha, 6.73%). Accordingly, these removal totals were divided into total forested land ownership to compute the “normalized” removal. The resulting removal percentages can be seen in Table 12 and Figure 24.

	<i>Private Industrial</i>	<i>Private Non-Industrial</i>	<i>Public</i>	<i>Total</i>
1986	33,976.04	82,400.89	315,651.62	432,028.55
1991	34,341.48	82,420.28	314,059.54	430,821.30
1996	33,076.54	79,044.77	311,400.68	423,522.00
2001	33,027.86	78,561.58	313,733.10	425,322.54
2006	31,064.89	78,265.99	313,875.85	423,206.74
2011	28,127.43	77,732.23	312,283.99	418,143.64

Table 11. Total forest area broken down by land ownership class and year

	<i>Private Industrial</i>	<i>Private Non-Industrial</i>	<i>Public</i>
1986-1991	1.18%	2.02%	1.98%
1991-1996	3.92%	4.37%	1.09%
1996-2001	1.04%	1.31%	0.24%
2001-2006	6.88%	1.22%	0.71%
2006-2011	12.80%	2.31%	1.10%

Table 12. Percentage of total forested land removed by ownership by 5-year interval

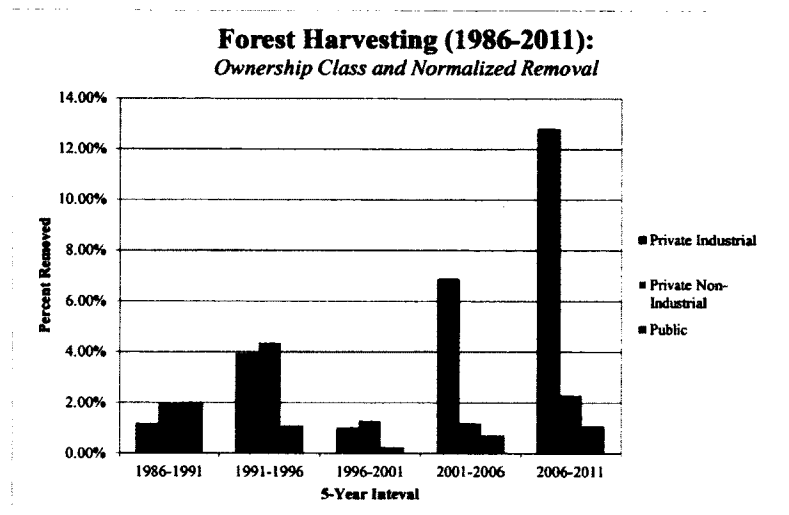


Figure 24. Percentage of total forested land removed by ownership by 5-year interval

The forest and non-forest change classification process not only yields change areas that suggest forest removal, but additionally forest areas that are regenerated (non-forest to forest). From the forest management perspective, this variable is in many ways as valuable, if not more so, than the harvesting totals. Accordingly, forest regeneration totals were calculated across the entire study area and, again, broken down by land ownership class. The results of these analyses can be seen in Table 13 and Figure 25. The total forest regeneration across all ownership classes does not take on any major trend in the positive or negative direction, with the exception of a steep decline in the 1991-1996 interval, which makes sense, given the heavy harvesting that occurred in that year. The ownership-specific trends, however, are of interest. For instance, again with the exception of 1991-1996, regeneration on public land has steadily declined. Conversely, both kinds of private land have seen somewhat steady growth in forest regeneration from the 1991-1996 interval to 2006-2011.

	<i>Private Industrial</i>	<i>Private Non-Industrial</i>	<i>Public</i>	<i>Total</i>
1986-1991	617.75	1,260.61	3,587.73	5,466.09
1991-1996	81.76	227.09	775.10	1,084.77
1996-2001	293.74	549.24	3,081.88	3,926.97
2001-2006	309.60	659.25	2,385.88	3,356.91
2006-2011	1,037.37	1,271.51	1,847.38	4,159.62

Table 13. Total regeneration by 5-year interval broken down by land ownership class

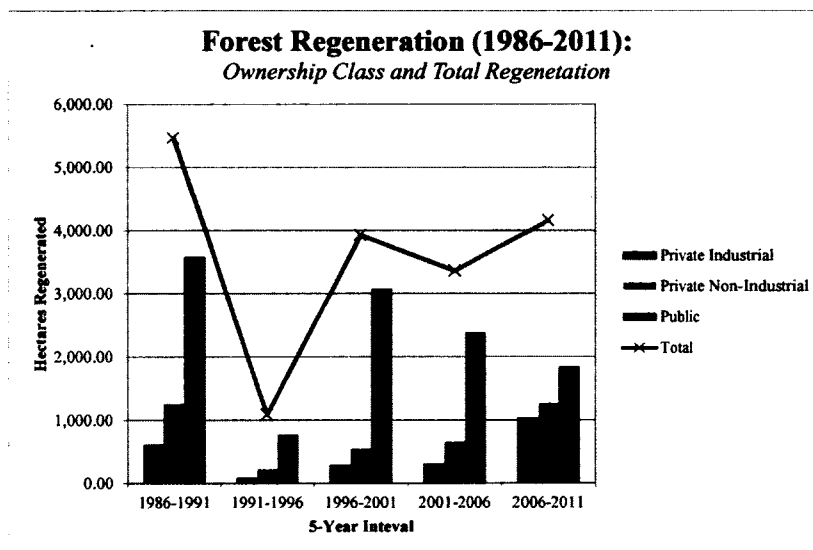


Figure 25. Total regeneration by 5-year interval broken down by land ownership class

These numbers, again, should be taken with the understanding of differential class-specific forest land ownership. Using the totals from Table 11, these regeneration values were normalized as a percent regeneration, rather than a raw total. The results can be seen in Table 14 and Figure 26. Generally speaking, a normalized regeneration (regeneration divided by total forest land ownership) of approximately 1% appears to be fairly common (average of all percentages = 0.87%). A major exception to this rule occurs, however, in the 2006-2011 interval, where private industrial land saw a 3.69%

regeneration and private non-industrial also had fairly high regeneration, with 1.64% overall.

	<i>Private Industrial</i>	<i>Private Non-Industrial</i>	<i>Public</i>
1986-1991	1.81%	1.54%	1.15%
1991-1996	0.25%	0.29%	0.25%
1996-2001	0.89%	0.70%	0.98%
2001-2006	1.00%	0.84%	0.76%
2006-2011	3.69%	1.64%	0.59%

Table 14. Percentage of total forested land regenerated by ownership by 5-year interval

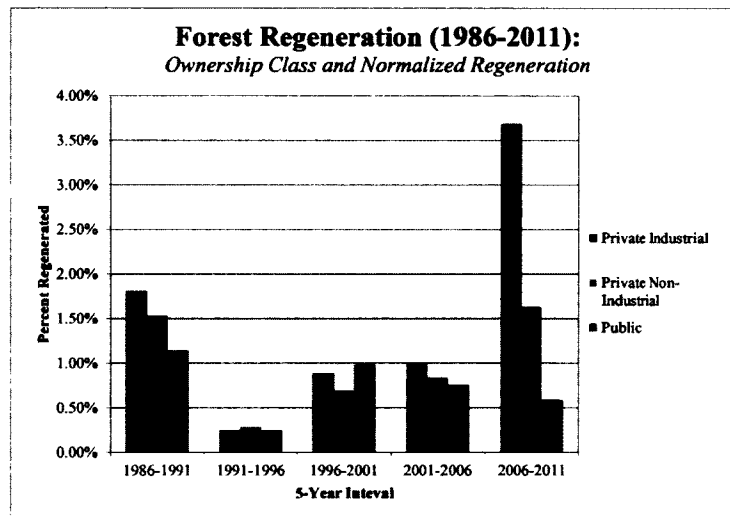


Figure 26. Percentage of total forested land regenerated by ownership by 5-year interval

The ability to estimate both forest harvesting and forest regeneration enables the combined analysis of long term forest management projections. Two metrics highlighting this ability were calculated. The first is a ratio of forest area harvested to forest area regenerated. In this scenario, a value of 1.0 would represent an equal amount of harvesting and regeneration has taken place throughout the 5-year interval. For each ownership class and temporal interval, this ratio was calculated. The results can be seen

in Table 15 and Figure 27. As can clearly be seen, only three class specific values were found to have ratios of 1 or less (as indicated by bolded value in Table 15), two of which belonged to public land and the other being private industrial. In general, the highest harvest-regeneration ratios are found on private industrial land, where between 1991 and 1996, for example, 16.47 times more forested land was harvested than regenerated. Conversely, the public lands appear to have the most consistently low harvesting ratios, with a peak between 1991 and 1996 of 4.43.

	<i>Private Industrial</i>	<i>Private Non-Industrial</i>	<i>Public</i>	<i>Total</i>
1986-1991	0.65	1.32	1.74	1.52
1991-1996	16.47	15.86	4.43	7.74
1996-2001	1.17	1.88	0.24	0.54
2001-2006	7.34	1.45	0.94	1.63
2006-2011	3.83	1.42	1.86	2.22

Table 15. Forest harvesting-regeneration ratio by ownership class by 5-year interval

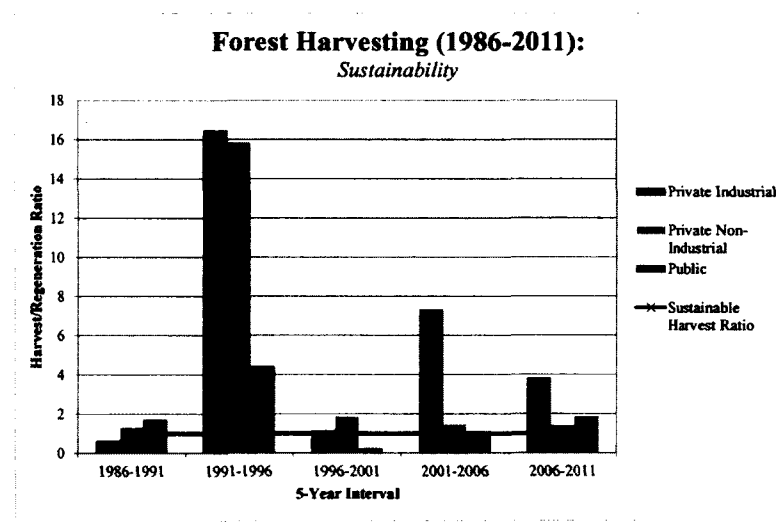


Figure 27. Ratio of forest harvesting to forest regeneration by 5-year interval broken down by ownership class

Another way to view this data is through the lens of net harvesting (or net regeneration, as the case may be). This value could be calculated using the raw totals (net harvesting in hectares) or the normalized totals (net harvesting in percent of total ownership), but again given the differential land ownership totals, percentages were deemed most comparably appropriate. The results of this analysis can be seen in Table 16. Clearly, public lands appear to have the most consistently low net forest harvesting totals, never exceeding 1%. Conversely, private industrial land appears to be, according to these data, on a negative long-term trajectory. For example, as Figure 28 highlights, if private industrial land were to continue its most recent net forest harvesting trajectory (9.11% net forest removal between 2006 and 2011), in 50 years there would only be 10,822 ha of the original 28,127 ha of forest left (38.47%). Conversely, looking at the same projections for public land, 95.11% of the original 312,284 ha of forested land would remain forested.

	<i>Private Industrial</i>	<i>Private Non-Industrial</i>	<i>Public</i>
1986-1991	-0.62%	0.49%	0.83%
1991-1996	3.67%	4.08%	0.84%
1996-2001	0.15%	0.61%	-0.74%
2001-2006	5.88%	0.37%	-0.05%
2006-2011	9.11%	0.67%	0.50%

Table 16. Net forest harvesting by 5-year interval broken down by ownership class

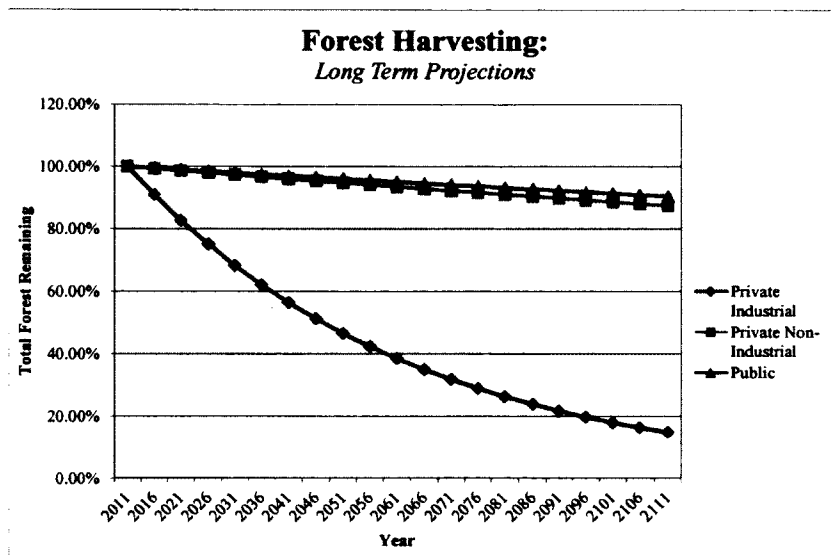


Figure 28. Long term total forest area projections based on 2006-2011 net forest harvesting percentages

CHAPTER IV

CONCLUSIONS

This study had a wide-ranging set of objectives, in terms of both remote sensing methods and real world application. Although the former played a more predominant role in the process, the latter provided the applicable justification for the methodological exploration. Operating under the paradigm of empiricism, this study took a largely exploratory approach to determining the optimal conditions for land cover classification and change detection. In incremental fashion, each procedure in the process was carefully vetted for resultant accuracy. Only when conditions were met to attain an acceptably high analytical accuracy was forward progress made. While the specific results of any remote sensing study are only immediately applicable to that study, certain broader trends can emerge upon which future analyses can be based. It is believed that the incremental approach used here can function not only as a framework for future investigation, but because the methods were explored using such a wide range of input parameters, a number of the specific results can help inform future research as well. Each set of significant findings will be discussed according to their specific applications below.

Segmentation Parameters

The impacts of the segmentation process on land cover classification are not to be ignored. The differences in resultant image classification accuracy performed with the range of segmentation parameters tested in this study highlighted this importance. While a number of studies exist that attempt to determine the optimal parameters for segmentation, this study utilized a purely empirical approach. There is a seemingly infinite combination of factors that can ultimately contribute to the determination of ideal segmentation parameters. These factors can be generally divided into two broad categories: (1) imagery characteristics and (2) project specifics. Within the former category, there a number of considerations including the image sensor type, spectral resolution, radiometric resolution, and spatial resolution. With an ever-increasing number of imagery types becoming available, these variables will only continue to complicate the segmentation process further. In terms of project specifics, the range of possibilities is even greater. Complicating factors may include desired land cover classification (number of classes, type and specificity of class definitions), study area characteristics (spatial extent, vegetation types, degree of urbanization, topography), temporal influence (single date image versus multitemporal analysis), and more. Accordingly, it is believed that an empirical approach, although perhaps more time consuming, is, at the current state of segmentation studies, one of the only approaches that can result in an objectively accurate image segmentation.

An important assumption was made in this study's segmentation parameter and resultant classification accuracy analysis. In both the pixel- and object-based scenarios, the training data segments (and for OBIA, the accuracy assessment segments as well)

were objectively assigned using pre-determined training sample unit centroids. Accordingly, it should be understood that perhaps in some cases the resulting segments did not precisely represent the classes they were intended to (See Figure 29 for visual explanation). In this figurative scenario, the desired sample unit was collected in the forested area. If the image was segmented at a relatively small scale (Segmented Image 1), the sample unit centroid assignment method would perform perfectly well. If this sample unit was a training sample, it would accurately train the model based on the desired forest classification. Likewise, if it was an accuracy assessment sample, its resultant assessment could be deemed an appropriate representation of ground conditions. In Segmented Image 2, however, which was segmented at a larger scale with perhaps less influence given to the color parameter, the resulting segments may no longer be representative of the ground conditions. As a result, this sample centroid, which was intended to represent purely forest, now assigned the entire segment to the forest classification, while on the ground it clearly overlaps a number of different cover types. As a result, the model would be trained with false information, and the accuracy assessment can no longer be deemed valid. The appropriate solution to this problem, and the manner by which training and accuracy samples *should* be determined in segmentation analyses, is through the selection of segments *themselves* as the sample units for each different combination of segmentation parameters. Given the total number of classifications performed (240) and large number of sample units used (540), however, this ideal process was not feasible for this study. It is believed that with an upper scale bound of 20 (segments are small enough), and an upper shape bound of 0.5 (segments are spectrally homogeneous enough), these mislabeling phenomena occurred scarcely

enough to still render the classifications and accuracy assessments valid. The very process of segmentation is, of course, intended to eliminate these false pixel groupings, but beyond a certain scale and with little influence given to spectral qualities of the imagery, false groupings could certainly occur and the assumptions used in this study could no longer be justified.

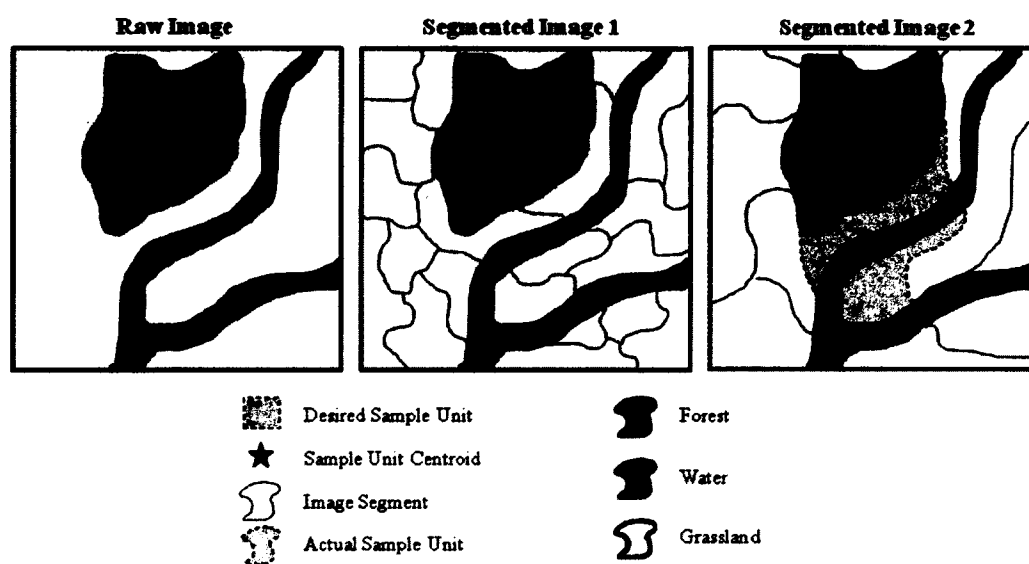


Figure 29. Figurative image segmentations and sample unit assignment

The results of the segmentation parameter analysis revealed a few key findings. First, and perhaps most obviously, the effect of the scale segmentation parameter had a direct and highly predictable effect on the resultant image segment size. While this finding may appear insignificant at face value, it forms a strong, quantitative basis for future studies using segmentation on Landsat 5 TM data. The scale parameter is primarily a factor of image spatial resolution (dictated further, of course, by the color and shape contributions as well). Accordingly, with the information provided in Figure 7,

one can determine an appropriate starting point for a similar Landsat-based segmentation. One hectare is equal to 10,000 m², or about 11 Landsat 5 TM pixels. If one is looking to, for example, study the distribution of different forest stand types and has a generic understanding of stand type spatial extent in hectares, one can use Figure 7 to determine an appropriate segmentation level, or at the very least a range of levels to test.

A second segmentation parameter finding is the effect of the scale parameter on segment size variability. As Figure 8 highlights, segmentations performed with very small scale parameters will have much more variably-sized segments than those at a "medium" size. The word "medium" is used, in this case, because when a Landsat scene with 30 m pixels is loaded into eCognition, the default scale parameter is set to 10. This variability is particularly important at a small scale parameter of 2, for example, where segments can be as small as a single pixel. Particularly in an OBIA environment, where a number of complex parameters can be estimated *per-segment* to train the classification model, such as band-specific means, standard deviations, skewness, and GLCM homogeneity, the different results from highly varied segment sizes can have drastic effects on these segment metrics. As segment size increases, however, this variation will have less of an effect, (even though beyond a scale of 8 segment size variation actually increases), because the data distributions *within* each segment will enable much more realistic and representative parameter calculations.

A third finding regarding the relationship between segmentation parameters and classification accuracy is perhaps that there was no finding at all. By this I mean that segmentation parameters alone could not predict resultant classification accuracies. Instead, the combination of analytical environment (pixel vs. object) and classification

algorithm (CART vs. Bayes) *in conjunction with* the segmentation parameters were the most indicative of resultant classification accuracy.

OBIA vs. Pixel-Based Classification

Since its emergence in the field of remote sensing in the 1990s, OBIA has primarily been used as a way to avoid misclassification of pixels due to noise introduced by high spatial resolution datasets. For these purposes, OBIA has proven fairly effective. Few studies, however, have documented the utility of using OBIA on medium resolution image datasets such as Landsat 5 TM. This absence is not without justification -- Landsat's 30 m pixels are, in many ways, image objects in their own right and have historically been very successful in land cover analyses of all kinds. For a land cover study conducted over a relatively small area with a fairly detailed classification scheme, a 30 m pixel may sufficiently reduce the spectral noise contained within an image to produce fairly accurate, functional ground units, despite their indiscriminant spatial placement. At the regional or landscape scale with more generalized classes such as this study, however, perhaps the noise reduction caused by grouping of pixels over large areas (OBIA) would produce a more desirable result. Again, it is believed that only through an objective, accuracy assessment-based empirical study can the question of pixel versus object be fully answered.

Interestingly, however, this study failed to determine outright whether pixel-based analysis or object-based analysis was preferable. Instead, like the segmentation parameters, the resultant classification accuracy depended much more heavily on the classification algorithm used. Across the entire range of scale and shape parameters,

Bayes pixel-based classification significantly outperformed Bayes object-based classification. Conversely, the relationship between CART pixel- and object-based classifications were much more linked to the segmentation parameters used. Hypotheses as to why these differences occurred will be discussed in the next section, CART vs. Bayes.

A discussion about the different uses of segmentation in pixel- and object-based environments which was mentioned first in METHODS should be expanded upon here. Some may approach this study with the question, "why is segmentation being used at all in a pixel-based environment?" And rightly so. The explanation is as follows. Typically in pixel-based analyses, training sample units are created through a process commonly referred to as region growing. In this process, an area of interest on the map is selected and a region is "grown" based on neighboring pixel values. The shape and extent of these regions are dictated by region growing properties that typically contain spectral and spatial limitations. In a multiresolution segmentation, however, the entire image is divided into small groupings and in bottom-up fashion, regions are "grown" objectively across the entire region based on scale, shape, color, compactness and smoothness parameters. As a result, instead of a group of subjectively selected and grown training samples, the segmentation process results in an array of *potential* samples that are distributed throughout the entire image. Accordingly, it is believed that not only is segmentation an effective method of training sample selection in a pixel-based environment, but perhaps it is even preferable to more traditional selection methods due to increased objectivity.

The same is true of training sample segments in OBIA. That being said, the uses of the segments themselves varies between OBIA and pixel-based analysis. In pixel-based analyses, the training samples are used simply to determine class-specific spectral means and variances. These values are ultimately compiled by class and then each pixel is classified individually based upon the probability that it belongs to a given class. How these probabilities are determined depends upon the specific classification algorithm (See CART vs. Bayes). In OBIA, however, any number of segment spectral and spatial parameters can be input into the training model (See METHODS for description of input parameters used in this study). This much more complex, multivariate training model is then applied to the remaining image segments. Additionally, in OBIA, the segments themselves can be used for accuracy assessment as well, whereas in a pixel-based environment, more traditional sample units are used. Accordingly, the segmentation process has much greater implications on the OBIA process than the pixel-based process.

CART vs. Bayes

The classification algorithm used in any land cover analysis is arguably one of the most important considerations throughout the entire process. While it is typically one of the latter steps in the image analysis process, it affects each and every step along the way, from classification scheme development to training sample selection, band selection and accuracy assessment. Historically there were two primary choices: supervised classification and unsupervised classification, the former involving a subjective training sample selection and objective classification, the latter involving objective image grouping and subjective classification. The emergence of OBIA in many ways eliminates

a great deal of the subjectivity involved in the process, ideally enhancing repeatability, increasing efficiency and resultant accuracy. That said, there are still a number of subjective choices to make in the OBIA process, one of which is the classification algorithm of choice. With the release of eCognition 8.7, a number of advanced classifier tools became available. These include *K*-Nearest Neighbor (KNN), Support Vector Machine (SVM), Decision Tree (CART), and Bayes. The latter two were selected for examination in this study due to their relative conceptual simplicity and yet their significant computational differences. Broadly defined, these two represent the differences between parametric (Bayes) and non-parametric (CART) classification methodologies. Quite simply, parametric statistics assume some predetermined (typically normal) distribution of the data, where non-parametric methods do not. While these differences are easy to comprehend theoretically, their computations in an image analysis environment become quite complex. Likewise, their results can be fairly difficult to assess. Despite this difficulty, a few clear trends emerged from the results of this study, and hypotheses will be made as to their potential causal mechanisms.

The single most interesting result from this study is the exceptional performance of the Bayes classifier. While it is not generally surprising that a parametric method would outperform a non-parametric method, the specific image characteristics used in this study make the Bayes accuracies particularly intriguing. The Bayes classifier assumes complete statistical independence of the input data in order to properly train the model with the parameters of interest and accurately classify the results. Typically in the case of a parametric classifier such as Bayes, one would perform a separability analysis (such as Jeffries-Matusita) or other image exploration techniques to determine a few

optimal bands for classification, rather than using the entire image. By limiting the number of bands used in the classification, you decrease the amount of covariance present in the input data, thereby increasing the matrix invertibility and facilitating the classification. As can be readily assumed, no such statistical independence was present in the input data used in this study. The 23 bands used for each year of the classification were made up of essentially two 10-band images roughly equivalent images at separate times of year (and 3 ancillary topographic datasets). Correlation and covariance values, in this scenario, are inherently high. While it may be perceived as user naivety to throw this many highly correlated bands into a parametric classification model, or perhaps technological naivety for eCognition to even allow such a process, the results nevertheless proved extremely accurate -- much more so than the more situationally "acceptable" non-parametric method, CART.

Given the fact that such a methodology, according to remote sensing tradition, is in many ways seen as conceptually and operationally irresponsible or even invalid, little research in the field exists to explore these anomalously high quality results. Interestingly, however, a variety of research within the statistical literature have found similar results, where the so-called "naive" Bayes classifier has performed exceptionally well despite high input data dependence -- "The word most used to describe its performance is "surprising" " (Kuncheva, 2006, pp.830). Rish (2001) found that the success of the naive Bayes classifier at predicting an accurate result was highest in two scenarios: (1) when input features were completely independent, as is expected by the model assumptions, and, interestingly, (2) when the features were entirely functionally dependent. In between these two extremes, the model performed poorly. Interestingly,

Kuncheva (2006) found that divergence measures (such as Matusita, a version of which is commonly used in digital image analysis), did not provide any insight into the performance of Bayes. In other words, the resultant classification accuracies acted independent of input feature divergence, which again stands in stark contrast to typical supervised classification processes. Kuncheva (2006) additionally speculated that mirrored covariances, such as those that would be present in the paired 10-band images used in this study, could potentially improve Bayes classifier accuracy. Additionally, Hand and Yu (2001) describe a study by Russek, Kronmal and Fisher (1983), where Bayes was actually outperformed by non-parametric methods when only 6 variables were included with the model, but when 22 variables were used, Bayes performed the best, defying the typical assumptions made in the remote sensing community.

Taking a closer look at the specific classification accuracies from Figure 10, we can start to make sense of these anomalous results. Most notable is the fact that Bayes pixel-based classification (BP) consistently outperformed Bayes object-based classification (BO). BP appeared to act fairly independently of training segment size, while BO had a generally positive relationship between increasing segment size and resultant accuracy. This can be explained by the differential parameters being used to train the classification model. In a pixel-based environment, as described earlier, only two parameters are being estimated: class-specific spectral means and variances. Accordingly, the combined training information can be assumed to result in a fairly consistent overall mean and variance value by class. With 50 training samples, it is believed that these values will be similar with both small and large training segment sizes. Additionally, with such broad and distinct land cover classes, these spectral

distributions are most likely very distinct from one another. As a result, even in the event of high covariance between bands, as long as the distributions agree with one another by band, the resulting accuracies should be fairly high. Conversely, in the object-based environment, a host of complex calculations are being made on each individual training object. At a very small segment size, these values are bound to have a wide array of distributions. For example, a skewness value for a segment size of 4 pixels for class *a* in segment *i* in band *x* may have a radically different value than that same class and band in segment *j* by mere virtue of having such a small sample size (4 pixels) from which to compute a fairly complex metric. Attempting to compile the wide range of values for skewnesses of class *a* in band *x* across all 50 training segments into a single distribution of classification probabilities will likely contain such a high overall variance that it would greatly overlap the same distribution for classes *b*, *c*, *d* and so on. With significantly larger segment sizes, however, these skewness values would likely become more consistent across class *a*, minimizing the variance of the class-wide skewness distribution and reducing overlap between that of classes *a*, *b*, *c* and so on. As a result, there would be less disagreement in the Bayes model between classes and a greater overall classification accuracy. Hand and Yu (2001) confirm this concept by stating, "[o]ne important reason [that the Bayes model performs well] is that it requires fewer parameters to be estimated than alternative methods which seek to model interactions in the individual class-conditional *x* distributions" (pp.387). In other words, when simpler parameters such as band-specific mean and variances (in the case of BP) are being estimated, as opposed to more complex parameters (such as those computed in BO), Bayes tends to perform well.

The results of the CART classifications are in some ways similar to those found in Bayes, particularly in terms of the relationship between CART pixel (CP), CART object (CO) and segment size. While Bayes compiles the information contained within each training segment to a single, band-specific distribution from which classification probabilities are assigned, CART maintains the unique characteristics of each individual segment and classifies accordingly. As such, CART is, in theory, much more sensitive to outlying data than Bayes. As a result, we see a similar relationship between CO and scale as was found in BO. At these small segment sizes, again, a variety of complex metrics are being calculated for each segment. Accordingly, we see a relatively low classification accuracy at a scale of 2 and fairly consistently increasing accuracies with greater scales.

Accuracy Assessment

This study was one of the first explorations of an area-based error matrix introduced by MacLean and Congalton (2012) for use in object-based land cover accuracy assessments. The purpose of any accuracy assessment is to determine the degree to which a land cover classification model has properly represented the ground conditions in thematic form using a representative and statistically robust sample dataset. The purpose of an error matrix, then, is to represent this information in graphical format from which specific accuracy estimations can be gleaned. Accordingly, in a pixel-based analysis, where each uniformly-sized pixel is classified individually, it makes sense then that the accuracy assessment be conducted with uniformly-sized sample units, each of which is given equal weight in the assessment. In object-based environments, however,

the end result of a land cover analysis is an array of polygons, typically varying in size from one to the next. As a result, misclassifications (and inversely, correct classifications), are not all equal in magnitude. If one were to misclassify a 10 ha polygon, for example, the effect on the overall image accuracy would be much greater than a 1 ha misclassification. The area-based error matrix seeks to account for these differences, and as such should be included in OBIA studies of all kinds.

To explore the implementation and implications of using such a methodology, each of the 120 object-based classifications performed in this study were assessed using both traditional and area-based error matrices. The results certainly highlight some definitive trends in terms of the differences and similarities in accuracy assessment techniques. Most notably, in every combination of segmentation parameters, image analysis environment (OBIA vs. pixel) and classification algorithm (CART vs. Bayes), with the exception of CART object-based at a shape of 0.5, the area-based accuracy assessment reported higher overall accuracies. In most cases, these differences were quite significant. A fairly simple hypothesis can be used to explain these differences. Segment size is a fairly good predictor of spectral homogeneity within a polygon. In other words, areas with fairly homogeneous land cover types, such as a vast tract of shrubland, will produce larger segments than very heterogeneous environments, such as urban areas, where smaller segment sizes will result. By the same token, an assumption can be made with a relatively high degree of confidence that larger polygons will be easier to classify correctly than smaller polygons -- a large tract of shrubland will be much easier for a classification algorithm to accurately classify than a smaller, highly variable environment. Accordingly, in such an area-weighted accuracy assessment, if we

assume that larger polygons are more likely to be classified correctly, then the resultant overall accuracies will be higher. For a quantitative account of this phenomenon, refer to Figure 10. At a small segmentation parameter, the variation in segment size is the largest. Likewise, with these high segment size variabilities, we see the largest absolute differences between traditional and area-based error estimations for both CART and Bayes, with the latter having the starker contrast of the two. At a scale of 2, segment sizes in a highly varied, more difficultly classified area, segment sizes can be as small as 1 pixel. A misclassification at this size will have little effect on the resultant accuracy assessment. However, the largest, presumably easiest to classify segments can have sizes of about 20 pixels, having a much greater impact on positively weighting the area-based matrix.

This increased area-based accuracy estimation phenomenon is believed to have a particularly strong effect on the classifications performed in this study, with such broad land cover classifications. The classes used in this study are not only broad in description, but very visually (and spectrally) distinct from one another. As a result, a large tract of forest can be relatively easily identified as such (i.e. a forest is a forest is a forest). However, if a more complex classification scheme was used, the positive effect of area-weighting may not be as great. If one were to try to decipher between different forest stand types within the broader classification, for example, the reverse might occur. The segment sizes would remain (because segmentation takes place independent of classification scheme), but a more complex classification scheme would presumably result in more misclassifications. These misclassifications may, in fact, negatively

weight the accuracy assessment. Further exploration would be needed to confirm or reject this idea.

In general, in the OBIA environment, it is believed that this area-based error matrix is a valuable metric to include in the accuracy assessment process. That being said, the user and producer of the land cover classification should be aware of the implications of such a methodology. In the end, both traditional and area-based accuracies should be reported to facilitate an unbiased but perhaps more insightful overall accuracy assessment.

Change Detection

In continuing with the paradigmatic approach of the rest of the study, the change detection analysis was performed on an empirical, accuracy assessment-dependent basis. Many methods exist for the detection and subsequent classification of land cover change over time. This study employed the tried and true method of single band differencing. Due to the simplicity of this method, a variety of tests were able to be performed. Additionally, with the broad classification utilized in this study, it was believed that single band differencing would be optimal for detecting significant forest cover changes. The change detection accuracy assessments produced definitive results that enabled the best subsequent image classifications.

This study introduced a new principal component-based change detection technique. Each of the 10 spectral and derivative bands from the late summer 2011 image were differenced from those same bands in 2006 and a principal components analysis was performed on the resultant 10-band difference image. The intention with

this methodology was to ideally capture as much of the change variation contained within those 10 separate bands into a single band, PC1, as possible. Although this method did not produce the highest accuracies, its results were intriguing nonetheless. At a class-specific change threshold of 2 SD, PC1 detected *the most* change out of any of the derivative bands (TC1, 2, 3, and NDVI) and as a result the most correctly classified change as well. However, in terms of omission errors, interestingly enough, it performed amongst the poorest of all 11 bands tested. In terms of overall performance, as estimated by Kappa, it notably outperformed NDVI, TC2 and raw bands 1-4. A qualitative, visual assessment of its change detection results reveals perhaps the most valuable finding. Although PC1 clearly fell short in identifying visibly distinct forest changes (clear cuts), it identified a number of other areas where more subtle forest changes occurred that most other bands failed to detect. With no ground information on what these changes actually represented, it is difficult to definitively state what occurred between 2006 and 2011 in these areas, but an educated visual approximation suggests that these areas underwent selective harvesting. That is, forested areas that were not clear cut but perhaps experienced a thinning process, resulting in density, basal area, and even species composition change were identified via PC1 and not in others. By virtue of the principal components analysis process, PC1 likely suffered (or perhaps benefitted, depending on the desired change type detection) from the amount of noise resulting from the inclusion of the entire range of spectral and derivative influence. In reducing the dimensionality of the 10 bands, it is entirely possible that starkly contrasting value changes may have cancelled one another out, resulting in a greater influence to those bands whose changes were more subtle. For instance, if a clear cut is indicated by a great increase in TC3 and

a great decrease in NDVI, these differences may be lost. Perhaps PC2 or PC3 might highlight some additional useful information absent in PC1.

Among all of the spectral and derivative bands tested at a change threshold of 2 SD, band 7 had the best overall change detection performance, with band 5 coming in at a close second. Overall performance was judged in two primary ways: Kappa and the tradeoff between change area user's and producer's accuracies. Kappa, being a single statistic, is relatively easy to compare, with band 7 having a higher Kappa than any other band. Change user's and producer's accuracies, however, are a bit more difficult. A judgment must be made between which is given a greater preference. Given the nature of the change-area classification method being used subsequent to the change detection, it was believed that a higher producer's accuracy (least errors of omission) was preferable. Accordingly, band 7 additionally had the highest producer's accuracy percentage.

Band 7 was selected for further analysis. Because its user's accuracy was higher than its producer's accuracy (more omission error than commission), it was thought that perhaps 2 SD was too large of a threshold. Accordingly, change thresholds were tested at intervals of 0.25 SD between 1 and 2. With almost equal, but slightly higher producer's accuracies (and the highest Kappa value), 1.75 SD was chosen as the best threshold for further use in classifying each interval back in time.

Interestingly, the change detection accuracies in previous intervals decline from that found in the 2006-2011 interval. While the range of Kappa values does not fall too far below 0.6 (2006-2011 Kappa 0.744), the tradeoff between user's and producer's accuracies are of particular interest. The tradeoff between user's and producer's accuracies for change area detection can be seen as over- or under-estimations of overall

change detection. With a very high change user's accuracy and low change producer's accuracy, it can be assumed that the model is greatly underestimating change areas. Conversely, high change producer's accuracies and low change user's accuracies suggest overestimation of change. In general, it would be desirable for these values to be equally high, but for the purpose of this study, as stated earlier, preference is given to slightly higher producer's accuracies -- leaning towards overestimation, rather than underestimation of change. As a result, we see that the 2006-2011 and 2001-2006 intervals are the only ones with desirable outcomes. For the other three intervals, the user's accuracies are significantly higher than the producer's accuracies, suggesting perhaps significant underestimation of change detection. This fact will be particularly important to keep in mind when analyzing the applied data and viewing the actual forest cover change totals for these intervals.

Such a decrease in change detection accuracy, to some extent, can be expected of the methodology used in this study. The explanation is as follows. The 2006-2011 interval change detection performed well, but certainly not perfectly. In fact, a 77.68% producer's accuracy suggests that as much as 22.32% of the change went undetected, even in this most accurate interval. Accordingly, only those areas classified as change were subsequently classified in terms of their 2006 land cover, as suggested by the C-CAP protocol. The 22.32% of change area that was not classified as such remained classified as its 2011 land cover, even though on the ground it most likely changed. Given the fact that change thresholds are determined on a class-specific basis, the misclassification of that 22.32% likely decreased the accuracy of the overall change mean and standard deviation values for the previous time interval. The change detection for

2001-2006, then, would suffer from this error. This process is repeated for each interval of interest ultimately leading to a compilation of error that, expectedly, results in steadily decreasing change detection accuracies. It is believed that in using such a change detection and classification methodology, these errors are unavoidable. Additionally, changes in forest harvesting practices can greatly hamper the model's ability to accurately detect change. If, for example, clear cutting was the harvesting practice of choice between 2001 and 2011 and selecting harvesting reigned supreme in previous years, the same change detection band and threshold values may no longer be reliable.

Forest Cover Change

Although this study was largely an exploration in remote sensing methods, the importance of applying these methods to specific, real-world phenomena should not be understated. The primary application of interest revolved around detecting and classifying changes in the forested environments of a two-county area in northeastern Oregon. The results highlight predominant trends in overall and ownership-specific changes in total forested area throughout this region over a 25-year time span at 5-year intervals. From this information two key indicators of forest management can be gleaned: forest harvesting and forest regeneration. Again, it should be reiterated that while many land cover changes may have occurred in this region beyond simple forest and non-forest classifications, the motivation for this study was to highlight changes specific to forested environments. These changes should be viewed, however, through the lens of the resultant single time land cover and change detection accuracies. As a

result, they should be taken not as absolute figures, but of estimations produced through a very specific series of methodological procedures.

Three predominant trends in forest harvesting practices emerge. The first relates to overall forest change, and the latter two revolve around ownership-specific trends. In terms of overall change, we see that the greatest amount of forest removal occurred in the most recent interval, 2006-2011. In total, 9,227 ha of forest were removed. This total decreases almost perfectly linearly to 1996-2001 where an estimated 2,127 ha of forest was removed. This total then climbs back up to a plateau for the intervals of 1986-1991 and 1991-1996 where 8,311 ha and 8,394 ha were removed, respectively. If we refer to an earlier discussion of change detection accuracies, however, we can clearly see how these figures may potentially be significantly higher in reality, as underestimation is a certain possibility during these intervals. With a change producer's accuracy of 56.74% between 1986 and 1991, it could be said that there was a 43.26% underestimation of total change. Making the potentially naive assumption that all of this underestimation should have been classified as forest to non-forest change (harvesting), the "real" total could be upwards of 14,000 ha. To make this assumption, however, would do a great disservice to the nature of the remote sensing analysis at hand and should, as a result, be only taken as pure speculation.

In addition to the overall forest harvesting trends, two ownership-specific trends emerge: (1) an increase in private industrial harvesting, and (2) an initial decrease in public land harvesting followed by a slower increase from 1986-2011. These trends are likely the result of a variety of factors. Speculation into the social, economic, and political mechanisms at work that have resulted in this shift from predominantly public

land harvesting to primarily private industrial warrants and entire geographic study in and of itself. As these subject matter-specific phenomena are not the primary motivation for this particular study, they will be largely left as fodder for further exploration. One important geospatial factor that is immediately relevant, however, is the fact that all timberlands are not equally harvestable. The ability to harvest timber from a given location in a forest depends primarily on three factors: (1) accessibility, (2) topography, and (3) rules and regulations. Accessibility is simply the ability for a logger to reach a given plot of timber – a factor that is controlled by the specific locations and densities of the forest road network. Closely related to accessibility is the quality of the terrain, or topography, of the timberlands. Some areas are simply too steep or otherwise impeded by natural, geologic features to harvest timber. And lastly, there are a variety of legislative and regulatory road blocks to a variety of logging operations, particularly relating to the preservation of wilderness and protection of endangered species. For instance, riparian environments are often protected against logging due to their importance in the preservation of certain fish species that could be harmed by increased runoff and/or other industrial pollutants thought to be caused by logging operations. Taking all of these factors together, a scenario can readily be imagined wherein private industrial timberlands, which tend to be on lower-lying elevations with less dramatic topography, having higher road densities and fewer regulatory impediments, are simply more harvestable than, for example, public lands. Accordingly, the comparative, ownership-specific trends that emerge in this study should be taken with the understanding that not all lands are equally harvestable.

Fortunately, there is an extant dataset that enables the comparison of ground data to the remote sensing estimates found in this study. The Oregon Department of Forestry collects information on an annual basis regarding forest management practices. One of the metrics that they collect is total timber board footage harvested, broken down by ownership class. Temporally, this information coincides nicely with the present study, being publicly and freely available for download from 1986-2010. The results of annual board footage harvested by ownership class can be seen in Figure 30. As can clearly be seen when comparing this study's results to the data shown below, there is a fair amount of disagreement. According to this information, public land harvesting has fairly precipitously declined since 1986 and has failed to recoup. Private industrial activity, however, appears to have maintained a fairly steady harvesting amount throughout the 25 year span.

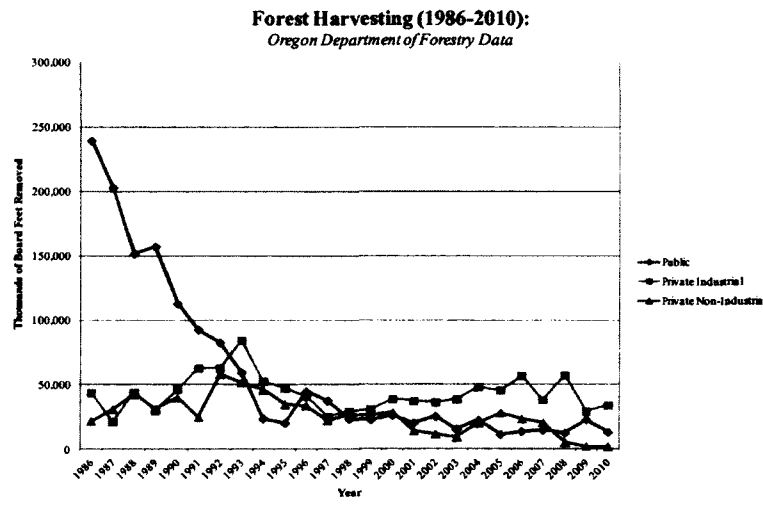


Figure 30. Forest harvesting data in board footage from Oregon Department of Forestry, 1986-2010

There are an exceedingly large number of possible explanations for these discrepancies, only a few of which will be discussed. First and foremost, it should be reiterated that the remote sensing totals should be taken as estimations perceived through the lens of the reported accuracies. Underestimation in early time intervals may account for some of these differences. Secondly, although certainly linked, board footage and total area removed are inherently two separate measures. Board footage takes not only area harvested into account, but a number of more specific tree-level variables, such as species, diameter and length. Additionally, board footage is a total measure of harvesting across a variety of management practices. This study was limited to identifying clear cutting operations only. Partial cuts and selective harvesting operations are less readily identified using Landsat imagery and were not feasible to explore in detail in this study, but are certainly included in board footage totals. Lastly, the ownership data used in this study were from 2011 tax parcel data. It was assumed that general ownership class has not changed in the past 25 years. This assumption, although significant, is believed to be largely valid in that public lands have been fairly stagnant in terms of their ownership and extent. Additionally, although there have been major changes in the specific companies, the private industrial land has primarily been exchanged from one logging company to the next, scarcely being purchased by non-industrial land owners or public entities. However, the ownership definitions made by the Oregon Department of Forestry may differ slightly from those used in this study, where perhaps the lines between private industrial and private non-industrial become slightly blurred.

LITERATURE CITED

- Adams, D. & G. Latta, 2003. Private timber harvest potential in Eastern Oregon. *OSU Forest Research Laboratory*, 42.
- Baatz, M. & A. Schäpe, 2000. Multiresolution segmentation: an optimization approach for high quality multi-scale image segmentation. In: *Angewandte Geographische Informationsverarbeitung*, J. Strobl, T. Blaschke and G. Griesebner (Eds.), Vol. 12, Wichmann-Verlag, Heidelberg, pp. 12-23.
- Blaschke, T., 2010. Object based image analysis for remote sensing. *ISPRS Journal of Photogrammetry and Remote Sensing* 65: 2-16.
- Blaschke, T., K. Johansen, & D. Tiede, 2011. Object-Based Image Analysis for Vegetation Mapping and Monitoring. In: *Advances in Environmental Remote Sensing: Sensors, Algorithms, and Applications*, Q. Weng (Ed.), Taylor & Francis, London, pp. 241-271.
- Breiman, L., J. Friedman, R. Olsen, & C. Stone, 1984. *Classification and Regression Trees*. The Wadsworth Statistics and Probability Series, Wadsworth International Group, Belmont, CA, 356 pp.
- Borak, J. & A. Strahler, 1999. Feature selection and land-cover classification of a MODIS-like data set for a semiarid environment. *International Journal of Remote Sensing* 20 (5): 919-938.
- Chander, G. & B. Markham, 2003. Revised Landsat-5 TM radiometric calibration procedures and postcalibration dynamic ranges. *IEEE Transactions on Geoscience and Remote Sensing* 41 (11): 2674-2677.
- Chavez, P., Jr., 1988. An improved dark-object subtraction technique for atmospheric scattering correction of multispectral data. *Remote Sensing of Environment* 24: 459-479.
- Chavez, P., Jr., 1996. Image-based atmospheric corrections -- revisited and improved. *Photogrammetric Engineering & Remote Sensing* 62 (9): 1025-1036.
- Civco, D., 1989. Topographic normalization of Landsat Thematic Mapper digital imagery. *Photogrammetric Engineering & Remote Sensing* 55 (9): 1303-1309.

- Cohen, W. & S. Goward, 2004. Landsat's role in ecological applications of remote sensing. *Bioscience* 54 (6): 535-545.
- Cohen, J., 1960. A coefficient of agreement for nominal scales. *Educational and Psychological Measurement* 20 (1): 37-40.
- Cohen, W., T. Spies, & M. Fiorella, 1995. Estimating the age and structure of forests in a multi-ownership landscape of western Oregon, USA. *International Journal of Remote Sensing* 16: 721-746.
- Congalton, R. & K. Green, 2009. *Assessing the accuracy of remotely sensed data: Principles and practices, Second Edition*, CRC Press, Boca Raton, FL, 208 pp.
- Congalton, R., R. Oderwald, & R. Mead, 1983. Assessing Landsat classification accuracy using discrete multivariate analysis statistical techniques. *Photogrammetric Engineering & Remote Sensing* 49 (12): 1671-1678.
- Coppin, P., I. Jonckheere, K. Nackaerts, B. Muys, & E. Lambin, 2004. Digital change detection methods in ecosystem monitoring: A review. *International Journal of Remote Sensing* 25 (9): 1565-1596.
- Crist, E. & R. Cicone, 1984. A physically-based transformation of Thematic Mapper data -- the TM Tasseled Cap. *IEEE Transactions on Geoscience and Remote Sensing* GE-22 (3): 256-263.
- Crist, E., R. Laurin, & R. Cicone, 1986. Vegetation and soils information contained in transformed Thematic Mapper data. In: *Proceedings of IGARSS '86 Symposium*: 1465-1470.
- Dobson, J., E. Bright, R. Ferguson, D. Field, L. Wood, K. Haddad, H. Iredale, J. Jensen, V. Klemas, R. Orth, & J. Thomas, 1995. NOAA Coastal Change Analysis Program (C-CAP): Guidance for regional implementation. *NOAA Technical Report NMFS 123*, U.S. Department of Commerce, Seattle, WA.
- Dorren, L., B. Maier, & A. Seijmonsbergen, 2003. Improved Landsat-based forest mapping in steep mountainous terrain using object-based classification. *Forest Ecology and Management* 183: 31-46.
- Espindola, G., G. Camara, I. Reis, L. Bins, & A. Monteiro, 2006. Parameter selection for region-growing image segmentation algorithms using spatial autocorrelation. *International Journal of Remote Sensing* 27 (14): 3035-3040.
- Fung, T. & E. LeDrew, 1988. The determination of optimal threshold levels for change detection using various accuracy indices. *Photogrammetric Engineering & Remote Sensing* 54 (10): 1449-1454.

- Gao, Y., P. Marpu, I. Niemeyer, D. Runfola, N. Giner, T. Hamill, & R. Pontius, Jr., 2011. Object-based classification with features extracted by a semi-automatic feature extraction algorithm -- SEaTH. *Geocarto International* 26 (3): 211-226.
- Geneletti, D. & B. Gorte, 2003. A method for object-oriented land cover classification combining Landsat TM data and aerial photographs. *International Journal of Remote Sensing* 24 (6): 1273-1286.
- Green, K., 2006. Landsat in context: The land remote sensing business model. *Photogrammetric Engineering & Remote Sensing* 72 (10): 1147-1153.
- Hand, D. & K. Yu, 2001. Idiot's Bayes: Not so stupid after all? *International Statistical Review* 69 (3): 385-398.
- Hantson, S. & E. Chuvieco, 2011. Evaluation of different topographic correction methods for Landsat imagery. *International Journal of Applied Earth Observation and Geoinformation* 13: 691-700.
- Healey, S., W. Cohen, Y. Zhiqiang, & O. Krankina, 2005. Comparison of Tasseled Cap-based Landsat data structures for use in forest disturbance detection. *Remote Sensing of Environment* 97: 301-310.
- Irons, J., J. Dwyer, & J. Barsi, 2012. The next Landsat satellite: The Landsat Data Continuity Mission. *Remote Sensing of Environment* In Press, 11 pp.
- Jensen, J., 2005. *Introductory digital image processing: A remote sensing perspective, Third Edition*, Pearson Prentice Hall, Upper Saddle River, NJ, 526 pp.
- Jobin, B., S. Labrecque, M. Grenier, & G. Falardeau, 2008. Object-based classification as an alternative approach to the traditional pixel-based classification to identify potential habitat of the grasshopper sparrow. *Environmental Management* 41: 20-31.
- Jordan, C., 1969. Derivation of leaf area index from quality of light on the forest floor. *Ecology* 50: 663-666.
- Kauth, R. & G. Thomas, 1976. The Tasseled Cap -- a graphic description of the spectral-temporal development of agricultural crops as seen in Landsat. In: *Proceedings of the Symposium on Machine Processing of Remotely Sensed Data, West Lafayette, Indiana, June 29-July 1, 1976*: 41-51.
- Kuncheva, L., 2006. On the optimality of Naive Bayes with dependent binary features. *Pattern Recognition Letters* 27: 830-837.

- MacLean, M. & R. Congalton, 2012. Map accuracy assessment issues when using an object-oriented approach. In: *Proceedings of the American Society for Photogrammetry and Remote Sensing 2012 Annual Conference*: 5 pp.
- Lau, C. & K. Hsiao, 2005. Bayesian classification for rice paddy interpretation. *The 23rd Asia Conference on Remote Sensing, Kathmandu, Nepal*, 7 pp.
- Lu, D., P. Mausel, E. Brondizio, & E. Moran, 2002. Assessment of atmospheric correction methods for Landsat TM data applicable to Amazon basin LBA research. *International Journal of Remote Sensing* 23 (13): 2651-2671.
- Lu, D., P. Mausel, E. Brondizio, & E. Moran, 2004. Change detection techniques. *International Journal of Remote Sensing* 25 (12): 2365-2407.
- Mas, J., 1999. Monitoring land-cover changes: a comparison of change detection techniques. *International Journal of Remote Sensing* 20 (1): 139-152.
- Masser, I., 2001. Managing our urban future: The role of remote sensing and geographic information systems. *Habitat International* 25: 503-512.
- Meyer, P., K. Itten, T. Kellenberger, S. Sandmeier, & R. Sandmeier, 1993. Radiometric corrections of topographically induced effects on Landsat TM data in an alpine environment. *ISPRS Journal of Photogrammetry and Remote Sensing* 48 (4): 17-28.
- Miller, R. & C. Small, 2003. Cities from space: Potential applications of remote sensing in urban environmental research and policy. *Environmental Science & Policy* 6: 129-137.
- Minnaert, M., 1941. The reciprocity principle in lunar photometry. *Astrophysics Journal* 93: 403-410.
- Möller, M., L. Lyburner, & M. Volk, 2007. The comparison index: A tool for assessing the accuracy of image segmentation. *International Journal of Applied Earth Observation and Geoinformation* 9: 311-321.
- Moran, M., R. Jackson, P. Slater, & P. Teillet, 1992. Evaluation of simplified procedures for retrieval of land surface reflectance factors from satellite sensor output. *Remote Sensing of Environment* 41: 169-184.
- Myint, S., M. Yuan, R. Cervený, & C. Giri, 2008. Comparison of remote sensing image processing techniques to identify tornado damage areas from Landsat TM data. *Sensors* 8: 1128-1156.

- Newman, M., K. McLaren, & B. Wilson, 2011. Comparing the effects of classification techniques on landscape-level assessments: pixel-based versus object-based classification. *International Journal of Remote Sensing* 32 (14): 4055-4073.
- Pradhan, R., M. Ghose, & A. Jeyaram, 2010. Land cover classification of remotely sensed satellite data using Bayesian and hybrid classifier. *International Journal of Computer Applications* 7 (11): 1-4.
- Radoux, J., P. Bogaert, D. Fasbender, & P. Defourny, 2011. Thematic accuracy assessment of geographic object-based image classification. *International Journal of Geographical Information Science* 25 (6): 895-911.
- Rasi, R., C. Bodart, H. Stibig, H. Eva, R. Beuchle, S. Carboni, D. Simonetti, & F. Achard, 2011. An automated approach for segmenting and classifying a large sample of multi-date Landsat imagery for pan-tropical forest monitoring. *Remote Sensing of Environment* 115 (12): 3659-3669.
- Riaño, D., E. Chuvieco, J. Salas, & I. Aguado, 2003. Assessment of different topographic corrections in Landsat-TM data for mapping vegetation types. *IEEE Transactions on Geoscience and Remote Sensing* 41 (5): 1056-1061.
- Ridd, M. & J. Liu, 1998. A comparison of four algorithms for change detecting in an urban environment. *Remote Sensing of Environment* 63: 95-100.
- Rish, I., 2001. An empirical study of the Naive Bayes classifier. In: Proceedings of the International Joint Conference on Artificial Intelligence, Workshop on Empirical Methods in A: 41-46.
- Rogan, J. & D. Chen, 2004. Remote sensing technology for mapping and monitoring land-cover and land-use change. *Progress in Planning* 61: 301-325.
- Rogan, J., J. Miller, D. Stow, J. Franklin, L. Levien, & C. Fischer, 2003. Land-cover change monitoring with classification trees using Landsat TM and ancillary data. *Photogrammetric Engineering & Remote Sensing* 69 (7): 793-804.
- Roughgarden, J., S. Running, & P. Matson, 1991. What does remote sensing do for ecology? *Ecology* 72 (6): 1918-1922.
- Russek, E., R. Kronmal, & L. Fisher, 1983. The effect of assuming independence in applying Bayes' theorem to risk estimation and classification in diagnosis. *Computers and Biomedical Research* 16: 537-552.
- Story, M. & R. Congalton, 1986. Accuracy assessment: A user's perspective. *Photogrammetric Engineering & Remote Sensing* 52: 397-399.

- Teillet, P., B. Guindon, & D. Goodenough, 1982. On the slope-aspect correction of multispectral scanner data. *Canadian Journal of Remote Sensing* 8 (2): 84-106.
- Treitz, P. & P. Howarth, 2000. Integrating spectral, spatial, and terrain variables for forest ecosystem classification. *Photogrammetric Engineering & Remote Sensing* 66 (3): 305-317.
- Treitz, P. & J. Rogan, 2004. Remote sensing for mapping and monitoring land-cover and land-use change -- an introduction. *Progress in Planning* 61: 269-279.
- Trimble, 2012. Trimble eCognition Developer 8.7 User Guide.
- Trimble eCognition Community, 2012. "Classifier Algorithm (CART, SVM, KNN, Bayes)." <URL: <http://www.ecognition.com/community>>.
- Tucker, C., 1979. Red and photographic infrared linear combinations for monitoring vegetation. *Remote Sensing of Environment* 8: 127-150.
- Wilson, E. & S. Sader, 2002. Detection of forest harvest type using multiple dates of Landsat TM imagery. *Remote Sensing of Environment* 80: 385-396.
- Wulder, M., R. Skakun, W. Kurz, & J. White, 2004. Estimating time since forest harvest using segmented Landsat ETM+ imagery. *Remote Sensing of Environment* 93: 179-187.
- Wulder, M., J. White, S. Goward, J. Masek, J. Irons, M. Herold, W. Cohen, T. Loveland, & C. Woodcock, 2008. Landsat continuity: Issues and opportunities for land cover monitoring. *Remote Sensing of Environment* 112: 955-969.
- Wulder, M., J. Masek, W. Cohen, T. Loveland, & C. Woodcock, 2012. Opening the archive: How free data has enabled the science and monitoring promise of Landsat. *Remote Sensing of Environment* In Press: 9 pp.
- Xian, G., C. Homer, & J. Fry, 2009. Updating the 2001 National Land Cover Database land cover classification to 2006 by using Landsat imagery change detection methods. *Remote Sensing of Environment* 113: 113-1147.

APPENDICES

APPENDIX A

UNION AND BAKER COUNTY LAND OWNERSHIP TOTALS

Counties	Total Area	United States Forest Service (USFS)						State of Oregon	Industrial	Non-Industrial	Other, Undetermined, or Water
		Total USFS	Bureau of Land Management (BLM)	Bureau of Reclamation (BR)	Department of Energy (DOE)	State of Oregon	Industrial				
Baker	7,990.38	2,616.38	2,462.40	76.01	1,461.36	2.63	14.04	36.52	41.92	3,807.81	9.92
Union	5,276.48	2,494.75	2,042.83	446.16	25.52	1.51	0.33	36.57	397.82	2,319.98	0.00
Total	13,267.06	5,111.13	4,505.23	522.17	1,486.88	4.14	14.37	73.10	439.74	6,127.79	9.92
Baker	100.00%	32.74%	30.82%	0.95%	18.29%	0.03%	0.18%	0.46%	0.52%	47.65%	0.12%
Union	100.00%	47.28%	38.72%	8.46%	0.48%	0.03%	0.01%	0.69%	7.54%	43.97%	0.00%
Total	100.00%	38.52%	33.96%	3.94%	11.21%	0.03%	0.11%	0.55%	3.31%	46.19%	0.07%

APPENDIX B

CHANGE DETECTION ACCURACY ASSESSMENTS BY BAND

Band 1 (Blue)

		Reference		Sum Area	User
Map			258.23	1,194.97	78.39%
		1,007.90		15,693.78	93.58%
	Sum Area	1,944.63	14,944.12	16,888.74	
	Producer	48.17%	98.27%		92.50%

Kappa = 0.558

Band 2 (Green)

		Reference		Sum Area	User
Map			210.36	1,184.98	82.25%
		970.00	15,703.76	15,703.76	93.82%
	Sum Area	1,944.63	14,944.12	16,888.74	
	Producer	50.12%	98.59%		93.01%

Kappa = 0.587

Band 3 (Red)

		Reference		Sum Area	User
Map			215.61	1,213.29	82.23%
		946.95	15,675.46	15,675.46	93.96%
	Sum Area	1,944.63	14,944.12	16,888.74	
	Producer	51.30%	98.56%		93.12%

Kappa = 0.596

Band 4 (Near Infrared)

		Reference		Sum Area	User
Map			416.02	445.54	6.63%
		1,915.10		16,443.20	88.35%
	Sum Area	1,944.63	14,944.12	16,888.74	
	Producer	1.52%	97.22%		86.20%

Kappa = -0.019

Band 5 (Shortwave Infrared 1)

		Reference		Sum Area	User
Map			339.81	1,751.97	80.60%
		532.47	14,944.30	15,136.78	96.48%
	Sum Area	1,944.63	14,944.12	16,888.74	
	Producer	72.62%	97.73%		94.84%

Kappa = 0.735

Band 7 (Shortwave Infrared 2)

		Reference		Sum Area	User
Map			348.30	1,772.07	80.34%
		520.86		15,116.67	96.55%
	Sum Area	1,944.63	14,944.12	16,888.74	
	Producer	73.22%	97.67%		94.85%

Kappa = 0.737

Normalized Difference Vegetation Index (NDVI)

		Reference		Sum Area	User
Map			227.26	1,397.63	83.74%
		774.26		15,491.11	95.00%
	Sum Area	1,944.63	14,944.12	16,888.74	
	Producer	60.18%	98.48%		94.07%

Kappa = 0.668

Principal Components Analysis (PC 1)

		Reference		Sum Area	User
Map			413.13	1,722.41	76.01%
		635.34		15,166.33	95.81%
	Sum Area	1,944.63	14,944.12	16,888.74	
	Producer	67.33%	97.24%		93.79%

Kappa = 0.679

Tasseled Cap Brightness (TC 1)

		Reference		Sum Area	User
Map			263.09	1,503.40	82.50%
		704.32	1,381.02	15,385.34	95.42%
	Sum Area	1,944.63	14,944.12	16,888.74	
	Producer	63.78%	98.24%		94.27%

Kappa = 0.688

Tasseled Cap Greenness (TC 2)

		Reference		Sum Area	User
Map			967.91	1,175.12	17.63%
		1,737.42		15,713.63	88.94%
	Sum Area	1,944.63	14,944.12	16,888.74	
	Producer	10.66%	93.52%		83.98%

Kappa = 0.050

Tasseled Cap Wetness (TC 3)

		Reference		Sum Area	User
Map			342.17	1,622.80	78.91%
		663.99		15,265.94	95.65%
	Sum Area	1,944.63	14,944.12	16,888.74	
	Producer	65.85%	97.71%		94.04%

Kappa = 0.685

APPENDIX C

BAND 7 CHANGE DETECTION ACCURACY ASSESSMENTS BY THRESHOLD

1.00 Standard Deviation

		Reference		Sum Area	User
Map					
				1,795.43	3,524.37
		215.68		13,364.37	98.39%
	Sum Area	1,944.63	14,944.12	16,888.74	
	Producer	88.91%	87.99%		88.09%

Kappa = 0.568

1.25 Standard Deviations

		Reference		Sum Area	User
Map					
				1,086.40	2,756.55
		274.48		14,132.19	98.06%
	Sum Area	1,944.63	14,944.12	16,888.74	
	Producer	85.89%	92.73%		91.94%

Kappa = 0.665

1.50 Standard Deviations

		Reference		Sum Area	User
Map					
				738.30	2,337.20
		345.73		14,551.54	97.62%
	Sum Area	1,944.63	14,944.12	16,888.74	
	Producer	82.22%	95.06%		93.58%

Kappa = 0.710

1.75 Standard Deviations

		Reference		Sum Area	User
Map			415.69	1,772.07	76.54%
		389.74		15,116.67	97.42%
	Sum Area	1,746.13	15,142.62	16,888.74	
	Producer	77.68%	97.25%		95.23%

Kappa = 0.744

2.00 Standard Deviations

		Reference		Sum Area	User
Map			348.30	1,772.07	80.34%
		520.86	14,995.81	15,116.67	96.55%
	Sum Area	1,944.63	14,944.12	16,888.74	
	Producer	73.22%	97.67%		94.85%

Kappa = 0.737

APPENDIX D

LAND COVER AREA TOTALS

Land Cover Type	Total Area by Year (ha)					
	1986	1991	1996	2001	2006	2011
Cropland	74,047.59	71,916.39	69,461.28	68,102.37	63,089.10	58,111.92
Developed	35,187.93	34,711.65	34,184.34	33,833.70	33,319.62	33,745.95
Forest	436,921.11	431,121.24	423,811.62	425,611.80	423,491.22	418,423.95
Grassland	237,302.10	243,075.24	250,282.44	248,088.33	252,782.19	260,583.39
Shrub/Scrub	365,914.44	368,560.44	371,649.78	373,690.89	376,799.85	378,588.51
Water	4,507.83	4,496.04	4,491.54	4,553.91	4,399.02	4,427.28

Land Cover Type	Area Increase or Decrease by Interval (ha)				
	1986-1991	1991-1996	1996-2001	2001-2006	2006-2011
Cropland	-2,131.20	-2,455.11	-1,358.91	-5,013.27	-4,977.18
Developed	-476.28	-527.31	-350.64	-514.08	426.33
Forest	-5,799.87	-7,309.62	1,800.18	-2,120.58	-5,067.27
Grassland	5,773.14	7,207.20	-2,194.11	4,693.86	7,801.20
Shrub/Scrub	2,646.00	3,089.34	2,041.11	3,108.96	1,788.66
Water	-11.79	-4.50	62.37	-154.89	28.26